10B.7 *A posteriori* subgrid-scale model tests based on the conditional means of subgrid-scale stress and its production rate

QINGLIN CHEN[1], MARTIN J. OTTE[2], PETER P. SULLIVAN[3], CHENNING TONG[1*]
Department of Mechanical Engineering
Clemson University, Clemson, South Carolina 29634

1. INTRODUCTION

Large eddy simulation (LES) computes the large, or resolvable scales of turbulent flows, and models the effects of the small, or subgrid (SGS) scales. When the filter is located in the inertial range, the energy-containing scales are well resolved and most of the turbulent stress is carried by the resolved scales. Under such conditions the LES result is to some extent insensitive to the subgrid-scale model employed (Nieuwstadt and de Valk (1987); Mason (1994)).

However, in LES of many important flows, such as in the near-wall region of a high-Reynolds-number turbulent boundary layer, the filter scale is inevitably in the energy-containing scales because the latter scale with the distance from the surface (Kaimal *et al.* (1972); Mason (1994); Peltier *et al.* (1996); Tong *et al.* (1998, 1999)). Consequently, a significant portion of the turbulent stress must be carried by the SGS model, causing strong dependence of the results on the SGS model (e.g., Mason and Thomson (1992); Sullivan *et al.* (1994); Tong *et al.* (1999); Porté-Agel *et al.* (2000*a*)). Any deficiencies in the SGS model are therefore likely to lead to errors in LES results in the near-wall region. For example, LES of the unstable ABL using the Smagorinsky model over-predicts the mean shear and the streamwise velocity variance (Nieuwstadt and de Valk (1987); Mason (1994); Sullivan *et al.* (1994); Khanna and Brasseur (1997)) in the surface layer, and at the same time underpredicts the vertical velocity skewness. These deficiencies in LES results have been argued to be related to the Smagorinsky model's being too dissipative (Mason (1994); Sullivan *et al.* (1994)). Various methods for improving LES results have been developed, including stochastic backscatter (Schumann (1975); Leith (1990); Mason and Thomson (1992)), the split model of Schumann (Schumann (1975); Sullivan *et al.* (1994)), a nonlinear model (Kosović (1997)), and the scale-dependent dynamic Smagorinsky model (Porté-Agel *et al.* (2000*a*)). The improvements achieved by these methods demonstrated the importance of incorporating surface-layer SGS physics into SGS models. However, a systematic understanding of the effects of model behaviors on LES results, i.e., how the SGS turbulence and SGS models affect the resolvable-scale statistics under these conditions, an important issue for improving SGS models, is still lacking.

Traditional *a priori* and *a posteriori* tests of SGS models (e.g., Clark *et al.* (1979); McMillan and Ferziger (1979); Bardina *et al.* (1980); Nieuwstadt and de Valk (1987); Piomelli *et al.* (1988); Lund and Novikov (1992); Mason and Thomson (1992); Domaradzki *et al.* (1993); Piomelli (1993); Härtel *et al.* (1994); Liu *et al.* (1994); Mason (1994); Meneveau (1994); Peltier *et al.* (1996); Juneja and Brasseur (1999); Sarghini *et al.* (1999); Tao *et al.* (2000); Porté-Agel *et al.* (2001); Sullivan *et al.* (2003)), although contributing greatly to our understanding of current SGS models, provide little information regarding the relationship between SGS models and LES results (statistics). From *a priori* tests it is difficult to predict the effects of model behavior on LES results, e.g., the correlation between the modeled and measured SGS stress components provides little information about model performance in simulations. From *a posteriori* tests it is difficult to relate deficiencies of LES results (e.g., the mean velocity and Reynolds stress profiles) to specific aspects of the model behavior. The two types of tests are disconnected as they deal with SGS stress and LES statistics, respectively. Therefore, *a priori* and *a posteriori* test results cannot be directly compared to further evaluate model performance.

To better understand the relationship between SGS models and LES statistics, as well as that between the SGS turbulence and the resolvable-scale statistics, a systematic *a priori* test approach was developed (Chen *et al.* (2003, 2005); Chen and Tong (2006)) based on the transport equations of the resolvable-scale velocity and velocity-scalar joint probability density function (JPDF). This approach analyzes the SGS dynamic terms that evolve the JPDF equation. The terms containing the SGS stress are the conditional SGS stress and the conditional SGS stress production rate conditional on the resolvable-scale velocity at the same location. The JPDF contains all single-point velocity statistics, thereby making it possible to relate model test results to LES statistics, i.e., to model performance in simulations.

Chen and Tong (2006) used this approach to study the SGS turbulence in the surface layer of the atmospheric boundary layer and identified several deficiencies of the SGS models that affect the LES statistics. The Smagorinsky model, the nonlinear model, the mixed model, and the Kosović nonlinear model were tested using measurement data from a convective atmospheric surface layer. They found that none of these models can predict both conditional SGS stress and conditional SGS stress production rate correctly at the same time. The Smagorinsky model and the Kosović nonlinear model

*Corresponding author. E-mail: ctong@ces.clemson.edu

under-predict the anisotropy and the variations of the level of anisotropy, which are considered to be important for predicting the mean shear and the streamwise velocity variance profile, whereas the nonlinear model and the mixed model over-predict both. The under-prediction of the vertical velocity skewness (Moeng (1984); Lemone (1990)) is argued to be related to the inability of the models to predict the asymmetry in the conditional production rate of the vertical velocity variance. Therefore, analyses using the JPDF equation can provide important guidance for developing SGS models. However, to evaluate the model performance in actual simulations, these conditional statistics need to be further examined in actual LES.

In the present work, a new *a posteriori* test approach is developed based on the transport equation of the resolvable-scale velocity JPDF to study the SGS stress models using LES data. The equation for the resolvable-scale velocity JPDF, f, was given by Chen *et al.* (2003) and Chen and Tong (2006):

$$\begin{aligned}\frac{\partial f}{\partial t}+v_j\frac{\partial f}{\partial x_j} &= \frac{\partial^2}{\partial v_i\partial x_j}\left\{\langle\tau_{ij}|\mathbf{u}^r=\mathbf{v}\rangle\, f\right\}\\ &+ \frac{\partial^2}{\partial v_i\partial v_j}\left\{\left\langle -\frac{1}{2}P_{ij}|\mathbf{u}^r=\mathbf{v}\right\rangle f\right\}\\ &+ \frac{\partial^2}{\partial v_i\partial x_i}\left\{\langle p^r|\mathbf{u}^r=\mathbf{v}\rangle\, f\right\}\\ &+ \frac{\partial^2}{\partial v_i\partial v_j}\left\{\left\langle p^r\frac{\partial u_j^r}{\partial x_i}|\mathbf{u}^r=\mathbf{v}\right\rangle f\right\}\\ &- \frac{g}{\Theta}\frac{\partial}{\partial v_3}\left\{\langle\theta^r|\mathbf{u}^r=\mathbf{v}\rangle\, f\right\}, \qquad (1)\end{aligned}$$

where $\tau_{ij}=(u_iu_j)^r-u_i^ru_j^r$ is the SGS stress (the Leonard stress $L_{ij}=(u_i^ru_j^r)^r-u_i^ru_j^r$ has been included in τ_{ij}) and $P_{ij}=-\left\{\tau_{ik}\frac{\partial u_j^r}{\partial x_k}+\tau_{jk}\frac{\partial u_i^r}{\partial x_k}\right\}$ is the SGS stress production rate. A superscript r and angle brackets $\langle.\rangle$ denote a resolvable-scale variable and an ensemble average. Θ and θ are the mean and fluctuating potential temperatures respectively.

The left-hand side of the equation is the time rate of change and advection in physical space. The right-hand side represents mixed transport in physical and velocity spaces by the conditional SGS stress and the resolvable-scale pressure and transport in velocity space by the conditional SGS stress production rate, the conditional resolvable-scale pressure-strain correlation, and the conditional buoyancy force. Equation (1.1) shows that the SGS stress directly affects the resolvable-scale velocity JPDF through the conditional SGS stress and the conditional SGS stress production and indirectly through the pressure terms. Therefore, the necessary conditions for LES to correctly predict the velocity JPDF are that the conditional means of SGS stress and SGS stress production rate must be reproduced by the SGS model (Chen *et al.* (2003)). Therefore, equation (1.1) provides a link between the SGS stress and the resolvable-scale velocity JPDF and can be used to study the effects of the SGS stress on the JPDF in *a posteriori* tests. In such tests the conditional means of LES-generated SGS stress and its production rate are compared to measurements and/or DNS.

We note that the *a posteriori* tests performed here are qualitatively different from traditional tests, in which the mean, variance, spectra and the profiles of other flow parameters are often compared with experimental measurements. (Direct comparisons between the instantaneous LES-generated SGS stress and measurements as done in the traditional *a priori* tests are not possible because LES fields are not correlated to the true turbulence fields). A major limitation of such *a posteriori* tests is that it is difficult to relate the deficiencies of LES results to specific aspects of the model behavior. This is because the SGS stress evolves LES fields through dynamic equations, which are chaotic with many degrees of freedom, making it difficult to relate the properties of the solutions to the behaviors of the SGS terms in the LES equations. By contrast, our *a posteriori* tests examine the conditional means, which evolve directly the resolvable-scale velocity and scalar statistics through the JPDF equation. Therefore, it provides a more direct link between the resolvable-scale statistics and the SGS models. In addition, traditional *a posteriori* test results generally cannot be directly related to *a priori* test results whereas the JPDF equation-based *a posteriori* tests analyze the same JPDF equation as the *a priori* tests, thereby making it possible to directly evaluate the consistency of model performance in the two types of tests.

In LES employing certain SGS models, such as the Smagorinsky model, only the deviatoric part of the SGS stress, $\tau_{ij}^d=\tau_{ij}-\frac{1}{3}\tau_{kk}\delta_{ij}$, is modeled. Therefore, it is also useful to examine the corresponding production term, P_{ij}^d, defined as (Chen and Tong (2006))

$$P_{ij}^d=-\left\{\tau_{ik}^d\frac{\partial u_j^r}{\partial x_k}+\tau_{jk}^d\frac{\partial u_i^r}{\partial x_k}\right\}. \qquad (2)$$

Thus, P_{ij} can be written as

$$P_{ij}=P_{ij}^d-\frac{2}{3}\tau_{kk}S_{ij}, \qquad (3)$$

where S_{ij} is the resolvable-scale strain rate tensor. Equation (1.3) shows that the normal components of P_{ij} contain the energy transfer rate from the resolvable to the subgrid scales, $P_{\alpha\alpha}^d$ ($\alpha=1,2,3$), and the redistribution rates among three normal components of the SGS stress (inter-component exchange), $-\frac{2}{3}\tau_{kk}S_{\alpha\alpha}$, respectively. The off-diagonal components of P_{ij} contain the production of SGS shear stress due to straining and rotation of the anisotropic part of SGS turbulence by the resolvable-scale velocity field, P_{ij}^d, and due to straining of the isotropic part of SGS turbulence, $-\frac{2}{3}\tau_{kk}S_{ij}, (i\neq j)$.

Chen and Tong (2006) studied the JPDF equation using field measurements data. They found that the results of $\langle\tau_{ij}|\mathbf{u}^r\rangle$ and $\langle P_{ij}|\mathbf{u}^r\rangle$ are closely related to the surface-layer dynamics. The updrafts generated by buoyancy, the downdrafts associated with the large-scale convective eddies, the mean shear, and the length scale inhomogeneity play important roles in the behaviors of $\langle\tau_{ij}|\mathbf{u}^r\rangle$ and $\langle P_{ij}|\mathbf{u}^r\rangle$. One important finding is

that each component of $\langle P_{ij}|\mathbf{u}^r\rangle$ is often dominated by only one SGS stress component and one resolved strain rate component. These results can be used to analyze the trend of the conditional SGS stress production rate predicted by SGS models, and to analyze the dynamics between the scalar flux and its production rate. We use this method to analyze the means and conditional means of the SGS stress and its production rate predicted in LES.

In this paper, the effectiveness of the new *a posteriori* test approach is evaluated by employing it to study SGS model performance using LES data. The rest of the paper is organized as follows. Section 2 outlines the LES and the field measurements. The means and conditional means of SGS stress and its production rate obtained in LES are compared with the measurements and *a priori* test results in section 3, followed by conclusions.

2. LES DATA AND FIELD MEASUREMENTS

In this work, several SGS models commonly employed in LES of the ABL, the Smagorinsky model (Smagorinsky (1963); Lilly (1967); Moeng (1984)), the split model (also called two-part eddy-viscosity model) (Sullivan *et al.* (1994)), and the Kosović model (Kosović (1997)) are used to generate LES fields for model testing. These models use the resolvable-scale strain rate (and the resolvable-scale rotation rate tensor for the Kosović model) as model inputs, representative of a class of SGS models. They have been widely employed in LES of the ABL and many researchers have extensive experience with them. In addition, these models are suitable for tests using the field measurement data (see below) and *a priori* tests have been conducted (Chen and Tong (2006)). Therefore, the tests will help elucidate the strengths and deficiencies of this class of models in terms of their ability to predict the resolvable-scale JPDF. We emphasize that the goal of the tests performed in the present paper is not to provide a comprehensive evaluation of the current SGS models but to demonstrate the proposed statistical *a posteriori* test approach by focusing on several commonly employed SGS models.

The data using the Smagorinsky model and the Kosović model are described by Otte and Wynngard (2001). The data using the split model are described by Sullivan *et al.* (1994). The split model (Sullivan *et al.* (1994)) preserves the usual eddy-viscosity model formulation, but includes a mean strain rate contribution and a reduced contribution from the fluctuating strain rate near the surface. Our previous *a priori* study (Chen and Tong (2006)) showed that the conditional statistics of the split model are similar to those of the standard Smagorinsky model, but with mean offsets and smaller magnitudes.

The Smagorinsky model is described in Smagorinsky (1963), Lilly (1967), Moeng (1984).

$$\tau_{ij}^{smg} = -2\nu_t S_{ij} = -2C_k \Delta e^{1/2} S_{ij}, \tag{4}$$

where $C_k = 0.1$, e, S_{ij}, and Δ are the model constant (Moeng (1984)), the SGS turbulent kinetic energy, the resolvable-scale strain rate, and the filter size, respectively. This variant of the model is due to Deardorff (1980). Chen and Tong (2006) used both formulations and found that the conditional statistics obtained are very close. Therefore, the properties of the Smagorinsky model are largely due to the proportionality of the modeled SGS stress and and the resolved strain rate. The split model was proposed by Sullivan *et al.* (1994):

$$\tau_{ij}^{split} = -2\nu_t \gamma S_{ij} - 2\nu_T \langle S_{ij}\rangle, \tag{5}$$

where γ is the isotropy factor, and ν_T is the mean field eddy-viscosity. These two factors change with height to match the Monin-Obukhov similarity theory at the first grid point and provide anisotropy in the SGS motion near the surface. In present study, we choose the second grid point to compute the mean and the conditional mean statistics, where the corresponding isotropy factor $\gamma = 0.61$. Kosović (1997) proposed a nonlinear model:

$$\begin{aligned}\tau_{ij}^{kos} &= -2\nu_t S_{ij} - (C_s\Delta)^2\{C_1(S_{ik}S_{kj} - \frac{1}{3}S_{mn}S_{mn}\delta_{ij}) \\ &\quad + C_2(S_{ik}\Omega_{kj} - \Omega_{ik}S_{kj})\},\end{aligned} \tag{6}$$

where Ω_{ij} is the rotation rate tensor and C_s, C_1, and C_2 are model parameters.

We note that LES results near the surface, where the errors are the largest, are influenced by both the SGS model and the boundary conditions. The latter might also have an influence on the LES conditional statistics. However, previous studies (See the introduction) have shown improvements in near-wall LES statistics with improved SGS models, indicating a strong role played by the SGS model. Therefore, we expect that *a posteriori* can provide valuable information on the SGS model performance. The issue of boundary conditions will be a topic of our future investigations.

The LES code used in the present investigation is well documented in the literature (Moeng (1984); Moeng and Wyngaard (1988); Sullivan *et al.* (1994, 1996); McWilliams *et al.* (1999); Otte and Wynngard (2001); Moeng and Sullivan (2002)). The spatial discretization is pseudospectral (Fourier) in the horizontal (x, y)-directions and finite difference in the vertical z-direction. The advective terms are implemented in rotational form and aliasing errors are controlled using an explicit sharp Fourier cutoff of the upper 1/3 wavenumbers Canuto *et al.* (1988). A staggered vertical mesh is used with the vertical velocity w and subgrid-scale energy e located at cell faces while the horizontal velocities (u, v), pressure p and potential temperature θ are located at cell centers. This grid arrangement maintains tight velocity-pressure coupling. The discretization and solution of the pressure Poisson equation is consistent with the time-stepping scheme and continuity equation and ensures that the flow remains incompressible Sullivan *et al.* (1996). The time stepping scheme is a third-order Runge-Kutta scheme (Spalart *et al.*, 1991; Sullivan *et al.*, 1996). Consistent with the horizontal Fourier representation, periodic boundary conditions are used on the sidewalls of the computational domain. At the lower boundary, wall functions are used to estimate the surface stress and temperature. The wall functions are

based on Monin-Obukhov similarity theory Businger *et al.* (1971) which incorporates stability effects in the logarithmic wind profile; an implementation is described by Moeng (1984). At the upper boundary of the domain a radiation condition Klemp and Durran (1983) is imposed along with zero subgrid-scale fields. A prognostic subgrid-scale turbulent kinetic energy equation including advection, buoyancy, diffusion, production and dissipation (Deardorff (1980)) is used to calculate the SGS eddy viscosity. Parallelization of the code is accomplished using the Message Passing Interface (MPI).

The parameters for the simulations are given in table 1. The ratio of the boundary layer depth, z_i, to the Monin-Obukhov length, $L = -u_*^3\Theta/k_a g\langle u_3'\theta'\rangle$, is close to -6, indicating moderately convective boundary layers, where $u_*^2 = -\langle u_1' u_3'\rangle$ (a prime denotes fluctuations), $k_a = 0.41$, and g are the friction velocity, the von Kármán constant, and the gravitational acceleration, respectively. The simulation results are compared with both the *a priori* test results and the results from measurements described in Chen and Tong (2006)).

The conditional statistics from the LES are compared with the results obtained using field measurement data. The field program, named the horizontal array turbulence study or HATS, was conducted at a field site 5.6 km east-northeast of Kettleman City, California, in the summer of 2000 as a collaboration primarily among the National Center for Atmospheric Research, Johns Hopkins University and Penn State University (C. Tong was part of the Penn State group). Horst *et al.* (2004) describe the field site and the data collection procedures in detail.

The design for the field measurements is based on the transverse array technique proposed, studied and first used by the Penn State group (Edsall *et al.* (1995); Tong *et al.* (1997, 1998, 1999)) for surface-layer SGS measurements in the ABL. The technique uses horizontal sensor arrays to perform two-dimensional filtering to obtain resolvable- and subgrid-scale variables. Two arrays are vertically spaced to obtain vertical derivatives. The primary horizontal array consists of nine equally spaced sonic anemometers (Campbell Scientific SAT3) and the secondary array has five sonics at a second height. The arrays are aligned perpendicular to the nominal prevailing wind direction.

The filter operation in the streamwise direction is performed by invoking Taylor's hypothesis. Filtering in the transverse direction is realized by averaging the output signals from the sonic arrays (Tong *et al.* (1998)). In the present study, we use the arrays to approximate top-hat filters, which are the most compact type in physical space and provide a good approximation of the LES filter. The LES filter is a combination of explicit filters (e.g., de-aliasing filter) and implicit filters (SGS model and numerical scheme). Although the simulations use a spectral cutoff filter in the horizontal directions for de-aliasing, the effective filter as a result of the dissipative nature of the SGS model has a slower roll-off (See Pope (2000) for a discussion of the filtering effects of the Smagorinsky model). In addition, the vertical derivatives are computed using center differencing, which is effectively a top-hat filter. Therefore, top-hat filters are a good approximation of the horizontal LES filter and provide consistency between the resolvable-scale velocity and its derivatives in the vertical direction.

5the resolvable scales need time to evolve to its "final" spectrum.

Four different array configurations are employed in the HATS program. The filter (grid) aspect ratio (Δ/z, where z as the height of the primary array) ranges from 0.48 to 3.88, allowing the effects of grid anisotropy to be examined. Chen and Tong (2006) focused on an unstable case from array 1, because it has the largest $\Delta/z = 3.88$, with highly anisotropic SGS motions and is thus the most difficult case for SGS models to predict. In the present work, we choose an unstable case from array 2, because its aspect ratio $\Delta/z = 2.0$ is closer to those of the LES data ($\Delta/z = 2.14$ for the split model runs and $\Delta/z = 1.92$ for the Smagorinsky model and the Kosović model runs) than the other arrays. The stability parameter $-z/L$ for this case is 0.36, larger than those for the LES fields at the second grid height (0.18 for the split model runs and 0.15 for the Smagorinsky model and the Kosović model runs). However, for an unstable boundary layer the influence of $-z/L$ essentially amounts to a stability correction, therefore is weaker that of Δ/z. Therefore, this difference is unlikely to significantly affect the comparisons. For more details of the HATS data, see Horst *et al.* (2004); Chen and Tong (2006).

Due to the complexity of the variables of interest and of the conditional sampling procedure, we are not able to provide a precise level of statistical uncertainty for the conditional statistics. However, by monitoring the statistical scatter while increasing the data size, we conclude that reasonable statistical convergence is achieved (Chen and Tong (2006)). Therefore, we believe that the data size is sufficient for obtaining reliable statistics for the analyses.

In the following section, the results for the mean SGS stress, $\langle\tau_{ij}\rangle$, and the conditional SGS stress, $\langle\tau_{ij}|\mathbf{u}^r\rangle$, are normalized by the square of the friction velocity u_*^2. The results for the mean and the conditional SGS stress production rates, $\langle P_{ij}\rangle$ and $\langle P_{ij}|\mathbf{u}^r\rangle$, are normalized by the estimated energy dissipation rate $\epsilon = \phi_\epsilon \frac{u_*^3}{k_a z}$, where $\phi_\epsilon = 1 - z/L$ for $z/L \leq 0$ as suggested by Kaimal *et al.* (1972).

3. Mean SGS stress and SGS stress production rate

As pointed out in the introduction, the SGS model predictions of the SGS stress and SGS stress production rate impact the LES statistics. In figures 1 and 2, the mean non-dimensional horizontal resolvable-scale velocity vertical gradient ($\Phi_m = \frac{\partial\langle u\rangle}{\partial z}\frac{k_a z}{u_*}$), the total velocity variances profiles, and the vertical resolvable-scale velocity skewness from the simulations are shown. Here Φ_m and the horizontal velocity variance are compared with an empirical form based on the Monin-Obukhov theory (Businger *et al.* (1971)) and the Minnesota data

(Lenschow and Stephens (1980)), respectively. The vertical resolvable-scale velocity skewness is compared with the skewness of the measured total vertical velocity (Lenschow and Stephens (1980); Wyngaard (1988)). This comparison is justified because the vertical velocity is reasonably well resolved beyond the first few grid points from the surface (Khanna and Brasseur (1997)) and the resolvable-scale statistics should approach those of the total velocity. The LES profiles obtained using the split model and the Kosović model are closer to measurements than those using the Smagorinsky model.

Table 2 shows that the measured Reynolds stress components $\langle u_1' u_1' \rangle$ and $\langle u_2' u_2' \rangle$ have larger values than the other components, so are the measured mean resolvable-scale stress components $\left\langle u_1^{r\prime} u_1^{r\prime} \right\rangle$ and $\left\langle u_2^{r\prime} u_2^{r\prime} \right\rangle$. This feature is generally captured by the all simulations. The smaller LES values for the normal components may be related to the difference in z_i/L between LES and measurements. We note that the properties of the SGS turbulence is strongly influenced by Δ/z. For a convective boundary layer the parameter z_i/L primarily influences the horizontal to vertical velocity variance ratio, the former having the largest contribution from eddies of the size of the boundary layer depth. For such a boundary layer the influence of z_i/L on the SGS turbulence is secondary to that of Δ/z. Therefore, the smaller LES values for the normal components will not significantly affect the results of the conditional SGS statistics.

The mean SGS stress normal components, $\left\langle \tau_{11}^d \right\rangle$ and $\left\langle \tau_{33}^d \right\rangle$, have larger magnitudes than $\left\langle \tau_{22}^d \right\rangle$. This feature cannot be captured by the Smagorinsky model and the split model because the strain rate components used to model τ_{11}^d and τ_{22}^d have zero mean. This situation is unlikely to be fundamentally different with the dynamic Smagorinsky model (Germano *et al.* (1991)) and its variants as they use the same the strain rate components. The Kosović model captures this trend much better, but slightly over-predicts $\left\langle \tau_{22}^d \right\rangle$ and $\left\langle \tau_{33}^d \right\rangle$. The better prediction is because this model can be derived from the SGS stress transport equation with a local equilibrium assumption and does not assume proportionality between the SGS stress and the resolvable strain rate. The mean SGS shear stress is under-predicted by all the models in both *a priori* and *a posteriori* tests. Because SGS model coefficients are usually constrained by the energy transfer rate, P_{kk}, there is no reason for the modeled mean SGS stress to match measurements. As previously pointed out (Kosović (1997); Chen and Tong (2006)), an under-prediction of $\langle \tau_{13} \rangle$ leads to over-predictions of the mean shear and the streamwise velocity variance (figure 1), which is further evidenced by the LES prediction of $\langle \tau_{13} \rangle$.

The mean SGS stress production rate components $\langle P_{11} \rangle, \langle P_{22} \rangle$, and $\langle P_{13} \rangle$ have larger magnitudes than the other components, which are generally captured by the models in both *a priori* and *a posteriori* tests. However, none of the models captures well the relative magnitudes among these components. The large magnitudes of $\left\langle P_{11}^d \right\rangle$ and $\left\langle P_{22}^d \right\rangle$ are generally captured by the models, but their ratio is not reproduced whereas $\left\langle P_{13}^d \right\rangle$ is under-predicted by the Smagorinsky model and the split model in both *a priori* and *a posteriori* tests, which is due to the under-prediction of $\left\langle \tau_{33}^d \right\rangle$ as $\left\langle P_{13}^d \right\rangle$ is dominated by $-\langle \tau_{33}^d \frac{\partial u_1^r}{\partial x_3} \rangle$ (Chen and Tong (2006)). At the same time, $\left\langle P_{13}^d \right\rangle$ is over-predicted by the Kosović model in both *a priori* and *a posteriori* tests due to its over-prediction of $\left\langle \tau_{33}^d \right\rangle$. The SGS production component $\left\langle P_{33}^d \right\rangle$ is well predicted in *a priori* tests by the Smagorinsky model and the split model but less well captured in the LES, which is probably due to the LES not reproducing the correct correlation between τ_{33}^d and $\partial u_3^r/\partial x_3$ (the dominant term in $\left\langle P_{33}^d \right\rangle$. See Chen and Tong (2006)).

In order to quantitatively measure the anisotropy of the SGS turbulence and the relationships among SGS components, we examine their eigenvalue structures using the Lumley triangle (Lumley (1978)). For example, the normalized mean SGS stress tensor for $\langle \tau_{ij} \rangle$,

$$\left\langle \tau_{ij}^d \right\rangle / \langle \tau_{kk} \rangle = \langle \tau_{ij} \rangle / \langle \tau_{kk} \rangle - \frac{1}{3}\delta_{ij}, \tag{7}$$

can be determined by two variables ξ and η defined in terms of its invariants (Pope (2000))

$$6\eta^2 = -2II = \left\langle \tau_{ij}^d \right\rangle \left\langle \tau_{ij}^d \right\rangle / \langle \tau_{kk} \rangle^2, \tag{8}$$

$$6\xi^3 = 3III = \left\langle \tau_{ij}^d \right\rangle \left\langle \tau_{jk}^d \right\rangle \left\langle \tau_{ki}^d \right\rangle / \langle \tau_{kk} \rangle^3, \tag{9}$$

where II and III are the second and the third invariants of the anisotropy tensor. If $\langle \tau_{ij} \rangle$ is isotropic, both ξ and η are zero (the first invariant or trace of $\left\langle \tau_{ij}^d \right\rangle$ is always zero by definition).

The Lumley triangle representations of the measured Reynolds stress and the resolvable-scale stress (figure 3(a)) show that both are close to axisymmetric with two large eigenvalues ($\eta = -\xi$). On the other hand, the mean SGS stress is close to axisymmetric with one large eigenvalue ($\eta = \xi$) in the surface layer. This difference is due to the influence of large-scale convective eddies, which result in large values of horizontal velocity variances. The filter near the surface removes the effects of the large-scale eddies, resulting in a structure close to axisymmetric with one large eigenvalue. The eigenvalue structure of the modeled mean SGS stress using these models (*a priori* tests), also shown in figure 3(a), is less anisotropic than the measurements. The slightly higher level of anisotropy of the Kosović model than that of the Smagorinsky model was also observed in *a priori* tests (Chen and Tong (2006)). The higher level of anisotropy of the split model than that of the Smagorinsky model is due to the contribution from the mean part of the modeled τ_{13} component.

The SGS stress production rate does not satisfy the Cauchy-Schwartz inequality. Consequently its ξ and η values are not confined to the Lumley triangle. Nonetheless, it is useful to present its structure using the Lumley triangle in order to compare it with that of the SGS stress. We use an arbitrary factor to normalize the production rate such that the ξ and η values fall within the

Lumley triangle. Therefore, $\xi > 0$ still represents a structure close to axisymmetric with one large eigenvalue, $\xi < 0$ represents a structure close to axisymmetric with two large eigenvalues, and the origin represent an isotropy structure. However, contrary to the case for SGS stress, the distance from the origin does not represent the level of anisotropy. Figures 3(c) and (d) show the Lumley triangle representation of the measured $\langle P_{ij} \rangle$ and $\langle P_{ij}^d \rangle$, respectively. Figure 3(c) shows that $\langle P_{ij} \rangle$ has a similar structure to the mean SGS stress as they are approximately on the same radical line originating from the origin, consistent with the good alignment and tensorial contraction between the conditional SGS stress and its production rate (Chen and Tong (2006)). Figure 3(d) shows that $\langle P_{ij}^d \rangle$ has a similar structure to $\langle P_{ij} \rangle$, but is closer to axisymmetric with one large eigenvalue ($\eta = \xi$), indicating that including the production rate due to straining of the isotropic part of the SGS stress shifts the SGS stress production rate structure away from being axisymmetric with one large eigenvalue. Note that in the *a priori* tests the modeled SGS stress is obtained by adding the measured $\tau_{kk}/3$ to the modeled τ_{ij}^d to compute the modeled P_{ij}. Therefore, the eigenvalue structure of the mean SGS stress production rate is influenced by the relative ratio between the measured $\tau_{kk}/3$ and the modeled τ_{ij}^d. We find that artificially increasing the percentage of τ_{kk} shifts the eigenvalue structure of the mean SGS stress production rate closer to being axisymmetric with two large eigenvalues.

The Lumley triangle representations of the Reynolds stress, the mean resolvable-scale stress, and the mean SGS stress obtained in LES using the Smagorinsky model, the split model, and the Kosović model are shown in figure 4(a), 5(a), and 6(a), respectively. The structures of the Reynolds stress and the mean resolvable-scale stress are well predicted by the split model and the Kosović model. The predicted level of anisotropy of the Reynolds stress using the Smagorinsky model is slightly lower than the measurements, but the resolvable-scale mean stress is slightly higher than the measurements, which results from the over-prediction of $\langle u_3' u_3' \rangle$ and the under-prediction of $\langle u_3^r u_3^r \rangle$ by the Smagorinsky model.

The LES mean SGS stress using the Smagorinsky model, the split model, and the Kosović model are close to axisymmetric with two large eigenvalues. Their eigenvalue structures are different from the measured mean SGS stress eigenvalue structure, but are similar to the *a priori* test results (figure 3(a)). The Lumley triangle representation of $\langle P_{ij} \rangle$ from LES is close to axisymmetric with one large eigenvalue (figure 4(b), 5(b), and 6(b)), which are similar to the measurements shown in figure 3(c). Its deviatoric part, $\langle P_{ij}^d \rangle$, is also close to axisymmetric with one large eigenvalue, similar to the measurements and the *a priori* test results (figure 3(d)), except the Kosović model, which over-predicts the magnitude of $\langle P_{22} \rangle$ due to the over-predicted magnitude of $\langle \tau_{22} \rangle$.

While the LES mean SGS stress eigenvalue structure is different from the measurements, the eigenvalue structures of the Reynolds and mean resolvable-scale stresses are quite well predicted, probably because the SGS stress has a relatively weak influence on the large convective eddies, which impact strongly the structure of the Reynolds stress. In order to examine the influence of the SGS model on the different parts of the resolved scales, we compute a band-passed stress using a band-pass filter ($\langle \tau_{ij}^b \rangle = \langle (u_i^r - u_i^{nr})(u_j^r - u_j^{nr}) \rangle$, where nr denotes a second low-pass filter of width n times that of the LES filter size. Figure 3(b) shows the LES results for several second filter widths ranging from 2 grid spaces to 34 grid spaces. For $n = 2$ the LES band-passed stress has a structure quite different from that of the measured band-passed stress. As the band width increases, i.e., as the large scales are included, the structure shifts closer to the mean resolvable-scale stress structure. Therefore, the LES stress structure near the filter scale quite different from that of measurements but the large scale LES structure is similar to the measurements, suggesting the SGS stress influences strongly the structure near the filter scale but not the large scales.

The different eigenvalue structures of the LES Reynolds stress and SGS stress can also be understood by examining the first two terms on the right-hand-side of equation (1.1): In a horizontally homogeneous atmospheric boundary layer, the derivatives in the horizontal directions in the first term vanish, and the SGS stress influences the resolvable-scale JPDF through $\langle \tau_{13} | \mathbf{u}^r \rangle$, $\langle \tau_{23} | \mathbf{u}^r \rangle$, and $\langle \tau_{33} | \mathbf{u}^r \rangle$. Therefore, the over-prediction of the magnitude of $\langle \tau_{22} \rangle$ by the Kosović model does not influence strongly the eigenvalue structure of the Reynolds stress. However, it may cause inaccuracies in flows that are not horizontally homogeneous. The slight inaccuracies in the LES eigenvalue structures of the Reynolds stress and the mean resolvable-scale stress using the Smagorinsky model come from the inaccuracies of $\langle u_3' u_3' \rangle$ and $\langle u_3^{r\prime} u_3^{r\prime} \rangle$, which are probably due to the inaccuracies of $\langle \tau_{33} \rangle$ (the dominant term in $\langle P_{33} \rangle$). The improvement of the LES results using the split model over the Smagorinsky model is probably a result of the increased anisotropy through $\langle \tau_{13} \rangle$, which partially compensates the effects of the under-prediction of τ_{33}. The second term in equation (1.1) contains the SGS stress production rate, which influences the resolvable-scale statistics regardless of homogeneity (Chen *et al.* (2003)). It is likely that the relatively good LES predictions of the eigenvalue structure of the Reynolds stress and the resolvable-scale stress are partly a result of the good prediction of the eigenvalue structure of $\langle P_{ij}^d \rangle$. In addition, the Lumley triangle representation of the normalized mean LES strain rate (normalized by $\sqrt{\langle \tau_{kk} \rangle / 2}/(0.1\Delta)$) is also generally well predicted by all models (figure 3(a), 4(a), 5(a) and 6(a)).

4. Conditional SGS stress and conditional SGS stress production

The conditional statistics are plotted against the sample-space variable for the horizontal resolvable-scale velocity, u_1^r, for different values of the vertical resolvable-scale velocity, u_3^r. To achieve sufficient statistical convergence while using relatively small data bin

sizes, we do not include the third velocity component as a conditioning variable. The data bins for the first conditioning variable [e.g., u_1^r in 7(a)] have the width shown in the figures (12 bins between ± 2 standard deviations whereas that for the second conditioning variable is twice as wide). For clarity, only the fluctuations of the resolvable-scale velocity components normalized by their respective r.m.s. values are plotted.

The measured conditional SGS stress and its production rate components are shown in figure 7. Their trends and the magnitudes generally depend on the resolvable-scale velocity and increase with the resolvable-scale velocity. One exception is $\langle P_{33}|u_1^r, u_3^r\rangle$, which weakly depends on u_1^r, consistent with the results in Chen and Tong (2006). The Lumley triangle representation, the eigenvector geometric alignment, eigenvalues, and the eigenvalue ratios of the conditional SGS stress to its production rate are shown in figures 8(a) and 9 respectively. These results are similar to those for array 1 discussed in detail in Chen and Tong (2006).

Several *a priori* test results for the Smagorinsky model are shown in figure 10. The model can predict well neither the conditional mean of SGS stress nor its production rate. It can only predict quite well the trends of some shear stress components, but not the normal components, and can predict the trends of some diagonal components of the conditional SGS stress production rate, but not the off-diagonal components. The magnitudes of these components are generally poorly predicted. The level of anisotropy is also severely under-predicted (figure 8(b)). These results are similar to those discussed in Chen and Tong (2006).

The *a priori* test results for the split model are generally similar to that of the Smagorinsky model except $\langle \tau_{13}|\mathbf{u}^r\rangle$ (figure 11) because the contribution from the mean part is generally small except for the SGS shear stress. Figure 11 shows that the variation of $\langle \tau_{13}^{split}|\mathbf{u}^r\rangle$ is smaller but the magnitude is larger than that of the Smagorinsky model due to the contribution from the mean part, which results in a higher level of anisotropy (figure 8(c)).

The results for the Kosović model (figure 12) show that it has better overall performance than the Smagorinsky model and the split model. Chen and Tong (2006) showed that it has the best overall performance among the models tested. However, it under-predicts the magnitude of the conditional SGS stress when the mean energy transfer is matched. The level of anisotropy (figure 8(d)) is also under-predicted, but the prediction is improved over that of the Smagorinsky model.

In the following we present the *a posteriori* test (LES) results of these SGS models and compare them with the measurements and the *a priori* test results discussed above (figure 7-12). Additional *a priori* test results can be found in Chen (2006).

4.1. The Smagorinsky model

Several LES results for $\langle \tau_{ij}^{smg}|u_1^r, u_3^r\rangle$ and $\langle P_{ij}^{smg}|u_1^r, u_3^r\rangle$ are shown in figure 13. The magnitudes of both are under-predicted. The trend of $\langle \tau_{11}^d|\mathbf{u}^r\rangle$ (not shown, refer to Chen (2006)) is generally well predicted. However, similar to the *a priori* test results, its magnitude is severely under-predicted. The trend and magnitude of $\langle \tau_{22}^d|u_2^r, u_3^r\rangle$ (not shown) are generally well predicted. The dependence of $\langle \tau_{33}^d|u_1^r, u_3^r\rangle$ (figure 13(a)) on u_1^r and the magnitude are under-predicted. Figure 13(b) shows that the trend of $\langle \tau_{13}|u_1^r, u_3^r\rangle$ on u_3^r is reasonably well predicted, but the magnitude is under-predicted. These results are similar to the *a priori* test results (figure 10). The under-prediction of $\langle \tau_{13}|u_1^r, u_3^r\rangle$ in both *a priori* and *a posteriori* tests provides strong evidence supporting the argument that it causes the over-prediction of the vertical mean shear and the streamwise velocity variance (See Chen and Tong (2006)).

The magnitude of $\langle P_{11}^d|u_1^r, u_3^r\rangle$ (not shown) is generally under-predicted, but its dependence on u_3^r is reasonably well predicted. The under-prediction of the magnitude is a result of the under-predictions of the magnitudes of τ_{11}^d and τ_{13}, the two dominant SGS stress components in $\langle P_{11}^d|u_1^r, u_3^r\rangle = \left\langle -\tau_{1j}^d \frac{\partial u_1^r}{\partial x_j}|u_1^r, u_3^r\right\rangle$ (Chen and Tong (2006)). The magnitude of $\langle P_{33}^d|u_1^r, u_3^r\rangle$ (figure 13(c)) and its asymmetric dependence on u_3^r are not well captured due to the under-prediction of τ_{33} because $\langle P_{33}^d|u_1^r, u_3^r\rangle$ is dominated by $\left\langle -\tau_{33}^d \frac{\partial u_3^r}{\partial x_3}|u_1^r, u_3^r\right\rangle$ (Chen and Tong (2006)). The trend and magnitude of $\langle P_{13}^d|u_1^r, u_3^r\rangle$ (figure 13(d)) are under-predicted. Again, this is due to the poor model prediction of $\langle \tau_{33}|u_1^r, u_3^r\rangle$ as it is also a dominant component in $\langle P_{13}^d|u_1^r, u_3^r\rangle$ (Chen and Tong (2006)). These results are similar to the *a priori* tests with the exception that the *a posteriori* results for $\langle P_{13}^d|u_1^r, u_3^r\rangle$ are somewhat better than the *a priori* test results. The poor prediction of $\langle P_{33}^d|u_1^r, u_3^r\rangle$, in particular its asymmetric dependence on u_3^r, in both *a priori* and *a posteriori* tests provides further evidence that it is the cause for the under-prediction of the vertical velocity skewness in the surface layer (figure 2. Also see Chen and Tong (2006)).

Chen and Tong (2006) argued that the level of anisotropy of the conditional SGS stress is very important for understanding the surface layer dynamics and for SGS modeling. The level of anisotropy of the conditional SGS stress can also be characterized by the representation in the Lumley triangle as done in Chen and Tong (2006). Previous results (Chen and Tong (2006)) have shown that the anisotropy is generally weak for negative u_3^r but is much stronger for positive u_3^r. For positive and negative u_1^r values $\langle \tau_{ij}|u_1^r, u_3^r\rangle$ is close to axisymmetric with one large eigenvalue and two large eigenvalues respectively, probably reflecting the shear and buoyancy effects. The level of anisotropy of the conditional SGS stress in LES represented in the Lumley triangle is shown in figure 14(a). Similar to the *a priori* test results, the data points are generally closer to the origin than the measurements, indicating an under-prediction of the level of the anisotropy. The qualitative dependence of the eigenvalue structure on the resolvable-scale velocity is not correctly predicted by LES. The

main reason for the under-prediction of the anisotropy is similar to that in *a priori* tests: the strong correlation between the modeled SGS stress and the resolved strain rate forces the reduction of the magnitude of the anisotropic (deviatoric) SGS stress when the correct energy transfer rate is maintained.

To study the relationship between the eigenvalue structures of the conditional SGS stress and its production rate, which is important for understanding the SGS dynamics and for SGS modeling, we examine the geometric alignment between $\langle \tau_{ij}^d | u_1^r, u_3^r \rangle$ and $\langle P_{ij}^a | u_1^r, u_3^r \rangle$ (where $P_{ij}^a = P_{ij} - P_{kk}\delta_{ij}/3$). We use the same definition of the measure of the geometric alignment given in Chen and Tong (2006). The eigenvalues of the conditional SGS stress tensor, $\langle \tau_{ij}^d | u_1^r, u_3^r, \rangle$, are denoted as α_τ, β_τ and γ_τ, ordered such that $\alpha_\tau \geq \beta_\tau \geq \gamma_\tau$, and the corresponding unit eigenvectors as $\vec{\alpha}_\tau, \vec{\beta}_\tau$ and $\vec{\gamma}_\tau$. Similarly, the eigenvalues of the conditional SGS stress production tensor, $\langle P_{ij}^a | u_1^r, u_3^r \rangle$, are denoted as α_P, β_P and γ_P, ordered such that $\alpha_P \geq \beta_P \geq \gamma_P$, and the corresponding unit eigenvectors as $\vec{\alpha}_P, \vec{\beta}_P$ and $\vec{\gamma}_P$. Three alignment angles, θ, ϕ and ξ, are defined as $\theta = \cos^{-1}(|\vec{\gamma}_P \cdot \vec{\gamma}_\tau|)$ (the angle between $\vec{\gamma}_P$ and $\vec{\gamma}_\tau$), $\phi = \cos^{-1}(|\vec{\beta}_P \cdot \vec{\beta}_\tau|)$, and $\xi = \cos^{-1}(|\vec{\alpha}_P \cdot \vec{\alpha}_\tau|)$. Chen and Tong (2006) found that $\langle \tau_{ij}^d | u_1^r \rangle$ and $\langle P_{ij}^a | u_1^r \rangle$ for array 1 are generally well aligned with the alignment angles less than 10° and weakly dependent on u_1^r while $\langle \tau_{ij}^d | u_3^r \rangle$ and $\langle P_{ij}^a | u_3^r \rangle$ are well aligned for positive u_3^r and less well aligned for negative u_3^r. The measurement results for array 2 are shown in figure 9.

The geometric alignment between $\left\langle \tau_{ij}^d | u_1^r, u_3^r \right\rangle$ and $\left\langle P_{ij}^a | u_1^r, u_3^r \right\rangle$ is generally well predicted in LES for by the Smagorinsky model (figure 15(a-b)) u_1^r and $u_3^r > 0$, but is over-predicted for $u_3^r < 0$. The generally good alignment for $u_3^r > 0$ indicates that the LES reproduces the effects of the quasi-equilibrium dynamics between the SGS stress production and destruction mechanism in the surface layer. But for $u_3^r < 0$, the LES still erroneously predicts a quasi-equilibrium state when the surface layer is not in such a state.

The trends of the eigenvalues of $\left\langle \tau_{ij}^d | u_1^r \right\rangle$ (figure 15(c-d)) are generally well predicted while the dependencies on u_3^r are generally less well predicted. At the same time the magnitudes are generally under-predicted, which is consistent with the results for $\left\langle \tau_{ij}^d | u_1^r, u_3^r \right\rangle$. The trends and the magnitude of the eigenvalue ratios of $\left\langle \tau_{ij}^d | u_1^r \right\rangle$ to $\left\langle P_{ij}^a | u_1^r \right\rangle$ (figure 15(e-f)) are not well predicted.

The overall similarity between $\langle \tau_{ij}^d | u_1^r, u_3^r \rangle$ and $\langle P_{ij}^a | u_1^r, u_3^r \rangle$ can be quantified using their contraction, $\langle \tau_{ij}^d | u_1^r, u_3^r \rangle \langle P_{ij}^a | u_1^r, u_3^r \rangle = \frac{\langle \tau_{ij}^d | u_1^r, u_3^r \rangle \langle P_{ij}^a | u_1^r, u_3^r \rangle}{|\langle \tau_{ij}^d | u_1^r, u_3^r \rangle| |\langle P_{ij}^a | u_1^r, u_3^r \rangle|}$. If the two tensors are perfectly aligned and their eigenvalues are proportional, the contraction has the value of one. The contraction (figure (16)) is predicted well for $u_3^r > 0$, but not for $u_3^r < 0$, consistent with the above eigenvector alignment and eigenvalue results.

The eigenvalue structure of the conditional SGS stress is studied here in the context of the resolvable-scale JPDF equation. Previous studies (e.g., Tao *et al.* (2000); Higgins *et al.* (2007)) have examined the alignment properties of the eigenvectors of the SGS stress and the resolved strain rate as well as other SGS and resolved variables. While the alignment of these eigenvectors are not directly related to the JPDF equation, the eigenvector alignment between SGS stress and resolvable-scale strain rate and between SGS stress and its production rate are useful for understanding the trend of the eigenvalue structures of the conditional SGS stress and the conditional SGS stress production rate. An investigation of the conditional alignment by the authors is under way and will be published in a separate paper.

The *a posteriori* results shown above are generally similar to the *a priori* test results, suggesting that the LES reproduces reasonably well the conditional resolvable-scale strain rate because these tests use the measured and LES conditional strain rates. However, there must be differences between the two types of test results for any imperfect SGS models as identical results would indicate that the model input (the resolvable-scale velocity gradient and the SGS kinetic energy, etc.) are perfectly predicted by LES, which would imply a perfect SGS model. Indeed, the better prediction of $\left\langle P_{13}^d | u_1^r, u_3^r \right\rangle$ in LES than in the *a priori* test results indicates that in certain situations the LES does not correctly reproduce the resolvable-scale stress and strain rate correlation. Nonetheless, the consistency between the *a posteriori* test results and the *a priori* test results demonstrates the effectiveness of analyzing the conditional SGS stress and its production rate as an approach for identifying specific model deficiencies and for evaluating SGS model performance in simulations.

4.2. The Split model

Table 2 shows that the LES results for the mean SGS stresses using the split model are essentially the same as those of the Smagorinsky model except the mean SGS shear stress component $\langle \tau_{13} \rangle$. The LES results for the conditional means for the two models are also similar except $\left\langle \tau_{13}^d | u_1^r, u_3^r \right\rangle$ (figure 17(a)). The dependence of $\left\langle \tau_{13}^d | u_1^r, u_3^r \right\rangle$ on u_1^r is under-predicted by the split model. The magnitude is also under-predicted and is smaller than that of the Smagorinsky model. The deviation of the *a posteriori* test results from the *a priori* tests and the measurements indicates that the dependencies of the flow statistics such as the strain rate on the resolvable-scale velocity are not correctly reproduced.

The LES conditional SGS stress production rate for the split model is less similar to that of the Smagorinsky model. The production component $\left\langle P_{11}^{split} | u_1^r, u_3^r \right\rangle$ (not shown) has a similar trend to that of the Smagorinsky model, but with a smaller magnitude due to the smaller magnitude of the predicted τ_{13}^d. The magnitude of $\left\langle P_{33}^{split} | u_1^r, u_3^r \right\rangle$ (figure 17(b)) is slightly smaller than that of the Smagorinsky model. The magnitude of $\left\langle P_{13}^{split} | u_1^r, u_3^r \right\rangle$ (figure 17(c)) is also slightly smaller than that of the Smagorinsky model. These differences further highlight the importance of the SGS stress produc-

tion rate (Chen *et al.* (2003)).

The Lumley triangle representation of the conditional SGS stress is shown in figure 14(b). Similar to the *a priori* test results, the data points are closer to the origin than the measurements, indicating an under-prediction of the level of the anisotropy. The geometric alignment (not shown) between the conditional SGS stress and conditional SGS stress production rate is generally similar to that of the Smagorinsky model except that the alignment angle θ and ξ are approximately five degrees larger. The generally good tensorial alignment indicates that the simulation reproduces the effects of the quasi-equilibrium dynamics between the SGS stress production and destruction rates in the surface layer for $u_3^r > 0$. However, the model also over-predicts the alignment for $u_3^r < 0$ when the surface layer is not in quasi-equilibrium, i.e., when there is an imbalance between the SGS stress production and destruction rates.

The eigenvalues and the eigenvalue ratios for the split model (not shown) are also similar to those of the Smagorinsky model, but with slightly smaller values. The tensorial contraction (figure 16) is also similar to that of the Smagorinsky model, but with sightly larger magnitudes.

These *a posteriori* results are similar to the *a priori* test results, not qualitatively different from that of the Smagorinsky model. Therefore, while the split model provides improvements over the Smagorinsky for some statistics, such as the mean shear and the streamwise velocity variance profile, it may be expected to have similar performance to the Smagorinsky model for other statistics.

4.3. The Kosović model

In LES the Kosović model predicts the overall trends of $\langle \tau_{ij}^d | u_1^r, u_3^r \rangle$ and $\langle P_{ij}^d | u_1^r, u_3^r \rangle$ (figure 18) well. The magnitude of $\langle \tau_{ij}^d | u_1^r, u_3^r \rangle$ is under-predicted while that of $\langle P_{ij}^d | u_1^r, u_3^r \rangle$ is better predicted. The trend of $\langle \tau_{11}^d | u_1^r, u_3^r \rangle$ (not shown) is generally well predicted, but the magnitude is under-predicted, similar to the *a priori* test results (Chen and Tong (2006)). The trend and magnitude of $\langle \tau_{22}^d | u_2^r, u_3^r \rangle$ (not shown) are well predicted while the magnitude of $\langle \tau_{33}^d | u_1^r, u_3^r \rangle$ (figure 18(a)) is slightly under-predicted. The trend of $\langle \tau_{33}^d | \mathbf{u}^r \rangle$ is generally well predicted but the dependence on u_3^r is over-predicted due to the over-prediction of the dependence on u_3^r of the conditional vertical gradient, $\langle \partial u_3^r / \partial x_3 | u_3^r \rangle$. The magnitude of $\langle \tau_{13}^d | u_1^r, u_3^r \rangle$ (figure 18(b)) is under-predicted by a factor of two. Its dependence on u_1^r is generally well predicted, but the dependence on u_3^r is under-predicted.

The magnitude of $\langle P_{11}^d | u_1^r, u_3^r \rangle$ (not shown) is under-predicted by a factor of two due to the under-prediction of the magnitude $\langle \tau_{13} | u_1^r, u_3^r \rangle$. The trend of $\langle P_{11}^d | u_1^r, u_3^r \rangle$ is generally well predicted and the magnitude of $\langle P_{33}^d | u_1^r, u_3^r \rangle$ (figure 18(c)) is generally well predicted, although the dependence on u_3^r is over-predicted because the dependence of $\langle \tau_{33}^d | u_1^r, u_3^r \rangle$ on u_3^r is over-predicted. The magnitude and trend of $\langle P_{13}^d | u_1^r, u_3^r \rangle$ (figure 18(d)) are well predicted, but the dependence on u_3^r is over-predicted due to the over-prediction of the dependence of $\langle \tau_{33} | u_1^r, u_3^r \rangle$ on u_3^r . These results are also similar to the *a priori* test results.

We note that in spite of the improved prediction of $\langle P_{33}^d | u_3^r \rangle$ by the Kosović model in both *a priori* and *a priori* tests, the vertical velocity skewness is under-predicted in LES (figure 2), suggesting that other SGS components (e.g., the pressure terms) may be causing the poor prediction. Therefore, while in most cases (e.g., the Smagorinsky model) the model predictions of $\langle \tau_{ij} | u_1^r, u_3^r \rangle$ and $\langle P_{ij} | u_1^r, u_3^r \rangle$ correspond well with LES results, there are exceptions. This result points to the need for further investigations of the JPDF equation, especially those that can lead to analytical results on the relationship between the SGS stress and the JPDF.

The Lumley triangle representation of the conditional SGS stress, shown in figure 14(c), is different from the measurements but is similar to the *a priori* test results. There are more data points close to $\eta = -\xi$ (axisymmetric with two large eigenvalues) than to $\eta = \xi$ (axisymmetric with one large eigenvalue), which comes from the over-prediction of the magnitude of $\langle \tau_{22}^d | u_1^r, u_3^r \rangle$. Again, the over-prediction of the magnitude of $\langle \tau_{22}^d | u_1^r, u_3^r \rangle$ is expected to have little consequence on the resolvable-scale statistics in a horizontally homogeneous boundary layer, but may result in inaccuracies in other flows where τ_{22} is important.

The geometric alignment angles between $\langle \tau_{ij}^d | u_1^r, u_3^r \rangle$ and $\langle P_{ij}^a | u_1^r, u_3^r \rangle$ are shown in figure 19(a) and (b). The alignment is generally well predicted for u_1^r and $u_3^r > 0$. The dependencies for $u_3^r < 0$ are less well predicted, but show improvements over the Smagorinsky model and the split model.

The dependencies of the eigenvalues of $\langle \tau_{ij}^d | u_1^r, u_3^r \rangle$ on u_1^r and u_3^r (figure 19(c) and (d)) are generally well predicted but their magnitudes are under-predicted. The trends and the magnitudes of the eigenvalue ratios (figure 19(e) and (f)) are not predicted correctly. The magnitude and the trend of the contraction between $\langle \tau_{ij}^d | u_1^r \rangle$ and $\langle P_{ij}^a | u_1^r \rangle$ shown in figure 16 are very close to the measurements and show significant improvements over the Smagorinsky model and the split model. These alignment results are similar to the *a priori* test results.

5. Conclusions

In this study a new *a posteriori* test approach is developed and employed to study SGS model performance. The approach compares the means of the LES-generated SGS stress and the SGS stress production rate conditional on the resolvable-scale velocity with measurements. These statistics must be reproduced by the SGS model for LES to correctly predict the one-point resolvable-scale velocity joint probability density function.

The measurement results represented in the Lumley triangle show that the Reynolds stress and the mean resolvable-scale stress are close to axisymmetric with two large eigenvalues, which is due to the influence of large convective eddies. The mean SGS stress is close

to axisymmetric with one large eigenvalue in surface layer, a result of the filter near the surface removing the contribution of these eddies. The mean SGS stress production rate has a similar structure to the mean SGS stress, consistent with the good alignment and tensorial contraction between the conditional SGS stress and its production rate (Chen and Tong (2006)).

The Lumley triangle representations of the LES mean SGS stress for all models are close to axisymmetric with two large eigenvalues, consistent with the *a priori* test results, but are different from the measured mean SGS stress eigenvalue structure. However, the LES Reynolds stress and the mean resolvable-scale stress using the split model and the Kosović model compare well with measurements. The predicted level of anisotropy of the Reynolds stress using the Smagorinsky model is slightly lower than the measurements, but that of the resolvable-scale mean stress is slightly higher than the measurements. The reasonably accurate prediction of the Reynolds stress structure is probably a result of the relatively weak influence of the SGS motions on the large convective eddies.

The magnitudes of the conditional SGS stress and the conditional SGS stress production rate are generally under-predicted in LES using the Smagorinsky model. The LES can reproduce the trends of some shear stress components but not those of the normal components, and can reproduce the trends of some normal components of the conditional SGS stress production rate, but not those of the off-diagonal components. The anisotropy of the conditional SGS stress is under-predicted. The geometric alignment and contraction between the conditional SGS stress and its production rate are generally reproduced for $u_3^r > 0$, but not for $u_3^r < 0$. The predictions of the trend of the conditional SGS stress using the dynamic Smagorinsky model and its variants are unlikely to be fundamentally different as they still assume proportionality between the SGS stress and the resolvable-scale strain rate. However, these models are not designed to provide the correct level of dissipation rate, therefore can result in LES statistics different from those of the Smagorinsky model. For example, the energy transfer rate from the resolvable to the subgrid scales due to the standard dynamic Smagorinsky model is lower than the correct level near the surface (e.g., Porté-Agel *et al.* (2000*b*)), resulting excessive resolvable-scale kinetic energy and shear stress. Consequently, the mean shear and the SGS shear stress are reduced so that the correct total shear stress is maintained as required by the large-scale conditions. Conceivably, there exists a value of the model constant that will produce the correct mean shear, but the model is unlikely to predict the correct level of energy transfer rate, resulting in inaccuracies in other resolvable-scale statistics such as the kinetic energy.

The results using the split model are similar to the *a priori* test results, and are not qualitatively different from that of the Smagorinsky model except the SGS shear component, τ_{13}. Therefore, the split model is expected to provide improvements over the Smagorinsky model for some LES statistics and to have similar performance for other statistics. The results using the Kosović model are similar to the *a priori* test results and show improvements over the Smagorinsky model.

The *a posteriori* test results discussed are generally consistent with the *a priori* test results. The model strengths and deficiencies observed here are also similar to those identified in our previous statistical *a priori* tests analyzing the conditional statistics (Chen and Tong (2006)). For example, the results provide further evidence that the over-predictions of the mean vertical shear and the streamwise velocity variance are a result of the under-prediction of the anisotropy of the SGS stress, and that the under-prediction of the vertical velocity skewness is caused by the under-prediction of the asymmetry of the conditional production rate of the vertical normal SGS stress.

The *a priori* and *a posteriori* tests conducted in the present study are based on the *necessary* conditions for the one-point resolvable-scale velocity JPDF given by Chen and Tong (2003). However, the consistency of the two types of test results observed in the present study suggests strongly that there is a close relationship between the *a priori* and *a posteriori* tests, which may be a result of the dynamics of turbulent flows. The strong empirical evidence of consistency also suggests that the *a priori* tests may be a good indicator of the *a posteriori* results and the model performance in LES, i.e., good *a priori* test results may be sufficient for good model performance in LES while poor *a priori* performance generally leads to poor *a posteriori* performance. Using the test results one can identify SGS model components that need improvements. For the models tested in the present study, the predictions of τ_{11}, τ_{13}, τ_{33}, and P_{33} need to be improved. Therefore, while mathematically the conditions given by Chen and Tong (2003) are necessary conditions, in the flows studied they also appear to be quite sufficient, further demonstrating the effectiveness of the approach of analyzing the conditional SGS stress and its production rate to test SGS models and to understand SGS physics.

The consistency between the *a priori* and *a posteriori* test results observed here is partly a consequence of the fact that both types of tests are based on the SGS terms in the velocity JPDF equation. By contrast the traditional *a priori* tests have no direct relationship to *a posteriori* tests because the former compare the instantaneous modeled and measured SGS stress and the latter compare the LES and measured statistics profiles. Our new analysis approach also provides direct tests of models for which the modeled SGS stress is not determined by the current resolved fields, such as transport-equation-based models (Hatlee and Wynngard (2007)). For these models the SGS stress is often not available *a priori*, making *a priori* tests impractical. However, the present *a posteriori* test approach can still be performed, allowing identification of specific model deficiencies and evaluation of SGS model performance in simulations. The present study demonstrates that analyses based on the conditional SGS stress and the conditional SGS stress production rate allow comprehensive model testing. It also provides impetus for further analytical study of the

JPDF equation, which will greatly enhance our understanding of the relationship between LES statistics and SGS models.

This work was supported by the National Science Foundation through grant No. ATM-0222421.

References

Bardina, J., J. H. Ferziger and W. C. Reynolds (1980). Improved subgrid scale models for large eddy simulation. *AIAA Paper 80-1357*.

Businger, J. A., J. C. Wynngard, Y. Izumi and E. F. Bradley (1971). Flux-profile relationships in the atmospheric surface layer. *J. Atmos. Sci.*

Canuto, C., M. Y. Hussaini, A. Quarteroni and T. A. Zang (1988). *Spectral methods in fluid dynamics*. Springer-Verlag.

Chen, Q. and C. Tong (2006). Investigation of the subgrid-scale stress and its production rate in a convective atmospheric boundary layer using measurement data. *J. Fluid Mech.* **547**, 65 – 104.

Chen, Q., D. Wang, H. Zhang and C. Tong (2005). Effects of subgrid-scale turbulence on resolvable-scale velocity-scalar statistics. *J. Turbulence* **6**, 36.

Chen, Q., H. Zhang, D. Wang and C. Tong (2003). Subgrid-scale stress and its production rate: conditions for the resolvable-scale velocity probability density function. *J. Turbulence* **4**, 027.

Chen, Qinglin (2006). Investigation of the effects of subgrid-scale turbulence on resolvable-scale statistics. PhD dissertation. Clemson University. Department of Mechanical Engineering.

Clark, R. A., J. H. Ferziger and W. C. Reynolds (1979). Evaluation of subgrid-models using an accurately simulated turbulent flow. *J. Fluid Mech.* **91**, 1–16.

Deardorff, J. W. (1980). Stratocumulus-capped mixed layers derived from a three-dimensional model. *Boundary Layer Met.* **18**, 495–527.

Domaradzki, J. A., W. Liu and M. E. Brachet (1993). An analysis of subgrid-scale interactions in numerically simulated isotropic turbulence. *Phys. Fluids A* **5**, 1747 – 1759.

Edsall, R. M., D. W. Thomson, J. C. Wyngaard and L. J. Peltier (1995). A technique for measurement of resolvable-scale flux budgets. In: *11th Symp. on Boundary Layers and Turbulence*. pp. 15 – 17. Amer. Meteor. Soc.. Charlotte, NC.

Germano, M., U. Piomelli, P. Moin and W. H. Cabot (1991). A dynamic subgrid-scale eddy viscosity model. *Phys. Fluids A* **3**, 1760–1765.

Härtel, C., L. Kleiser, F. Unger and R. Friedrich (1994). Subgrid-scale energy-transfer in the near-wall region of turbulent flow. *Phys. Fluid* **6**, 3130 – 3143.

Hatlee, S. C. and J. C. Wynngard (2007). Improved subfilter-scale models from the hats field data. *J. Atmos. Sci.*

Higgins, C. W., C. Meneveau and M. B. Parlange (2007). The effect of filter dimension on the subgrid-scale stress, heat flux, and tensor alignments in the atmospheric surface layer. *J. Atmos. Ocean. Tech.* **24**, 360–375.

Horst, T. W., J. Kleissl, D. H. Lenschow, C. Meneveau, C.-H. Moeng, M. B. Parlange, P. P. Sullivan and J. C. Weil (2004). Hats: Field observations to obtain spatially-filtered turbulence fields from transverse arrays of sonic anemometers in the atmosperic surface flux layer. *J. Atmos. Sci.* **61**, 1566 – 1581.

Juneja, A. and J. G. Brasseur (1999). Characteristics of subgrid-resolved-scale dynamics in anisotropic turbulence, with application to rough-wall boundary layers. *Phys. Fluid* **11**, 3054 – 3068.

Kaimal, J. C., J. C. Wyngaard, Y Izumi and O. R. Coté (1972). Spectral characteristic of surface-layer turbulence. *Q.J.R. Met. Soc.* **98**, 563 – 589.

Khanna, S. and J. G. Brasseur (1997). Analysis of monin-obukhov similarity from large-eddy simulation. *J. Fluid Mech.* **345**, 251 – 286.

Klemp, J. B. and D. R. Durran (1983). An upper boundary-condition permitting internal gravity-wave radiation in numerical mesoscale models. *Mon. Wea. Rev.* **111**, 430–444.

Kosović, B. (1997). Subgrid-scale modelling for the large-eddy simulation of high-reynolds-number boundary layer. *J. Fluid Mech.* **336**, 151 – 182.

Leith, C. E. (1990). Stochastic backscatter in a subgrid-scale model: plane shear mixing layer. *Phys. Fluids A* **2**, 297 – 299.

Lemone, M. A. (1990). Some observations of vertical velocity skewness in the convective planetary boundary-layer. *J. Atmos. Sci.* **47**, 1163 – 1169.

Lenschow, D. H. and P. L. Stephens (1980). The role of thermals in the convective boundary layer. *Bound.-Layer Meteor.* **19**, 509 – 532.

Lilly, D. K. (1967). The representation of small-scale turbulence in numerical simulation experiments. *In Proc. IBM Scientific Computing Symp. Environ. Sci.* p. 195.

Liu, S., C. Meneveau and J. Katz (1994). On the properties of similarity subgrid-scale models as deduced from measurements in a turbulent jet. *J. Fluid Mech.* **275**, 83–119.

Lumley, J. L. (1978). Computational modeling of turbulent flows. *Adv. Appl. Mech.* **18**, 123 – 176.

Lund, T. S. and E. A. Novikov (1992). Parametrization of subgrid-scale stress by the velocity gradient tensor. *Annual Research Briefs - Center for Turbulence Research* pp. 27 – 43.

Mason, P. J. (1994). Large-eddy simulation: A critical review of the technique. *Quart. J. Roy. Meteor. Soc.* **120**, 1–26.

Mason, P. J. and D. J. Thomson (1992). Stochastic backscatter in large-eddy simulation of boundary layers. *J. Fluid. Mech.* **242**, 51 – 78.

McMillan, O. J. and J. H. Ferziger (1979). Direct testing of subgrid-scale models. *Am. Inst. Aeronaut. Astronaut. J.* **17**, 1340 – 1346.

McWilliams, J. C., C-H. Moeng and P. P. Sullivan (1999). Turbulent fluxes and coherent structures in marine boundary layers: Investigations by large-eddy simulation. In: *Air-Sea Exchange: Physics, Chemistry, Dynamics, and Statistics* (G. Geernaert, Ed.). pp. 507–538. Kluwer.

Meneveau, C. (1994). Statistics of turbulence subgrid-scale stress: Necessary conditions and experimental tests. *Phys. Fluids* **6**, 815.

Moeng, C.-H. (1984). Large-eddy simulation model for the study of planetary boundary-layer turbulence. *J. Atmos. Sci.* **41**, 2052 – 62.

Moeng, C. H. and J. C. Wyngaard (1988). Spectral analysis of large-eddy simulations of the convective boundary layer. *J. Atmos. Sci.* **45**, 3573–3587.

Moeng, C-H. and P. P. Sullivan (2002). Large-eddy simulation. In: *Encyclopedia of Atmospheric Sciences* (J. R. Holton, J. Pyle and J. A. Curry, Eds.). pp. 1140–1150. Academic Press.

Nieuwstadt, F. T. M. and P. J. P. M. M. de Valk (1987). A large eddy simulation of of buoyant and non-buoyant plume dispersion in the atmospheric boundary layer. *Atmos. Environ.* **21**, 2573 – 2587.

Otte, M. J. and J. C. Wynngard (2001). Stably strasified interfacial-layer turbulence from large-eddy simulation. *J. Atmos. Sci.*

Peltier, L. J., J. C. Wyngaard, S. Khanna and J. Brasseur (1996). Spectra in the unstable surface layer. *J. Atmos. Sci.* **53**, 49 – 61.

Piomelli, U. (1993). High reynolds-number calculations using the dynamic subgrid-scale stress model. *Phys. Fluid A* **5**, 1484 – 1490.

Piomelli, U., P. Moin and J. H. Ferziger (1988). Model consistency in large eddy simulation of turbulent channel flows. *Phys. Fluid* **31**, 1884 – 1891.

Pope, S. B. (2000). *Turbulent Flows*. Cambridge University press. Cambridge, England.

Porté-Agel, F., C. Meneveau and M. Parlange (2000*a*). A scale-dependent dynamics model for large-eddy simulation: application to a neutral atmospheric buoyancy layer. *J. Fluid Mech.* **415**, 261 – 284.

Porté-Agel, F., M. B. Parlange, C. Meneveau and W. E. Eichinger (2001). A priori field study of the subgrid-scale heat fluxes and dissipation in the atmospheric surface layer. *J. Atmos. Sci.* **58**, 2673–2698.

Porté-Agel, F., M. B. Parlange, C. Meneveau, W. E. Eichinger and M. Pahlow (2000*b*). Subgrid-scale dissipation in the atmospheric surface layer: Effects of stability and filter dimension. *J. Atmos. Sci.* **57**, 75–87.

Sarghini, F., U. Piomelli and E. Balaras (1999). Scale-similar models for large-eddy simulations. *Phys. Fluids* **11**, 1596–1607.

Schumann, U. (1975). Subgrid scale model for finite difference simulations of turbulent flows in plane channels and annuli. *J. Comp. Physics* **18**, 376 – 404.

Smagorinsky, J. (1963). General circulation experiments with the primitive equations: I. the basic equations. *Mon. Weather Rev.* **91**, 99 – 164.

Spalart, P. R., R. D. Moser and M. M. Rogers (1991). Spectral methods for the navier-stokes equations with one infinite and 2 periodic directions. *J. Comp. Phys.* **96**, 297–324.

Sullivan, P. P., J. C. McWilliams and C.-H. Moeng (1994). A subgrid-scale model for large-eddy simulation of planetary boundary-layer flows. *Boundary-Layer Met.* **71**, 247 – 276.

Sullivan, P. P., J. C. McWilliams and C. H. Moeng (1996). A grid nesting method for large-eddy simulation of planetary boundary-layer flows. *Boundary Layer Met.* **80**, 167–202.

Sullivan, P. P., T. W. Horst, D. H. Lenschow, C.-H. Moeng and J. C. Weil (2003). Structure of subfilter-scale fluxes in the atmospheric surface layer with application to large-eddy simulation modeling. *J. Fluid Mech.* **482**, 101 – 139.

Tao, B., J. Katz and C. Meneveau (2000). Geometry and scale relationships in high reynolds number turbulence determined from three-dimensional holographic velocimetry. *Phys. Fluids* **12**, 941 – 944.

Tong, C., J. C. Wyngaard and J. G. Brasseur (1999). Experimental study of subgrid-scale stress in the atmospheric surface layer. *J. Atmos. Sci.* **56**, 2277–2292.

Tong, C., J. C. Wyngaard, S. Khanna and J. G. Brasseur (1997). Resolvable- and subgrid-scale measurement in the atmospheric surface layer. In: *12th Symp. on Boundary Layers and Turbulence*. pp. 221 – 222. Amer. Meteor. Soc.. Vancouver, BC, Canada.

Tong, C., J. C. Wyngaard, S. Khanna and J. G. Brasseur (1998). Resolvable- and subgrid-scale measurement in the atmospheric surface layer: technique and issues. *J. Atmos. Sci.* **55**, 3114–3126.

Wyngaard, J. C. (1988). Structure of the pbl. In: *Lectures on Air Pollution Modeling*. p. 385. Amer. Meteor. Soc.. Boston.

Case	$L_x, L_y \times L_z$	$N_x, N_y \times N_z$	Q_*	U_g	u_*	$-z_i/L$
Sullivan 1994	10000×2000	250×128	0.1	20.0	0.66	5.63
Otte 2001 (Smag)	2500×999	144×160	0.2	15.0	0.66	6.04
Otte 2001(Kosović)	2500×1000	140×160	0.2	15.0	0.65	5.57

Table 1: LES simulation parameters

	HATS	*a priori*			LES		
		Smag	Split	Kosović	Smag	Split	Kosović
$\langle u_1' u_1' \rangle / u_*^2$	12.12				5.08	5.79	4.80
$\langle u_2' u_2' \rangle / u_*^2$	13.19				4.52	5.15	4.47
$\langle u_3' u_3' \rangle / u_*^2$	1.86				1.43	1.20	0.89
$\langle -u_1' u_3' \rangle / u_*^2$	1.00				0.84	0.98	0.82
$\langle u_1^{r\prime} u_1^{r\prime} \rangle / u_*^2$	9.78				3.76	4.96	3.39
$\langle u_2^{r\prime} u_2^{r\prime} \rangle / u_*^2$	11.40				3.20	4.31	3.16
$\langle u_3^{r\prime} u_3^{r\prime} \rangle / u_*^2$	0.44				0.12	0.38	0.25
$\langle -u_1^{r\prime} u_3^{r\prime} \rangle / u_*^2$	0.46				0.39	0.71	0.52
$\langle \tau_{11}^d \rangle / u_*^2$	0.55	0.014	0.011	0.32	0.006	0.003	0.29
$\langle \tau_{22}^d \rangle / u_*^2$	-0.08	0.012	0.026	0.05	0.006	0.006	0.19
$\langle \tau_{33}^d \rangle / u_*^2$	-0.44	0.007	0.008	-0.33	-0.012	-0.009	-0.48
$\langle -\tau_{13} \rangle / u_*^2$	0.57	0.225	0.376	0.23	0.444	0.278	0.29
$\langle \tau_{kk}/3 \rangle / u_*^2$	1.87				1.318	0.831	1.12
$\langle P_{11} \rangle / \epsilon$	0.87	0.67	0.75	0.69	1.13	0.80	0.64
$\langle P_{22} \rangle / \epsilon$	0.29	0.44	0.42	0.46	0.18	0.27	0.32
$\langle P_{33} \rangle / \epsilon$	0.07	0.09	0.08	0.03	-0.04	0.00	0.02
$\langle -P_{13} \rangle / \epsilon$	0.63	0.90	0.90	0.53	1.34	0.60	0.32
$\langle P_{11}^d \rangle / \epsilon$	0.80	0.59	0.67	0.62	1.10	0.79	0.60
$\langle P_{22}^d \rangle / \epsilon$	0.19	0.34	0.32	0.36	0.15	0.24	0.30
$\langle P_{33}^d \rangle / \epsilon$	0.11	0.12	0.11	0.07	0.04	0.06	0.09
$\langle P_{13}^d \rangle / \epsilon$	0.22	-0.05	-0.05	0.32	0.00	0.02	0.43

Table 2: Statistics from the HATS (array 2) data, the *a priori* tests, and the LES (at the second grid-point height).

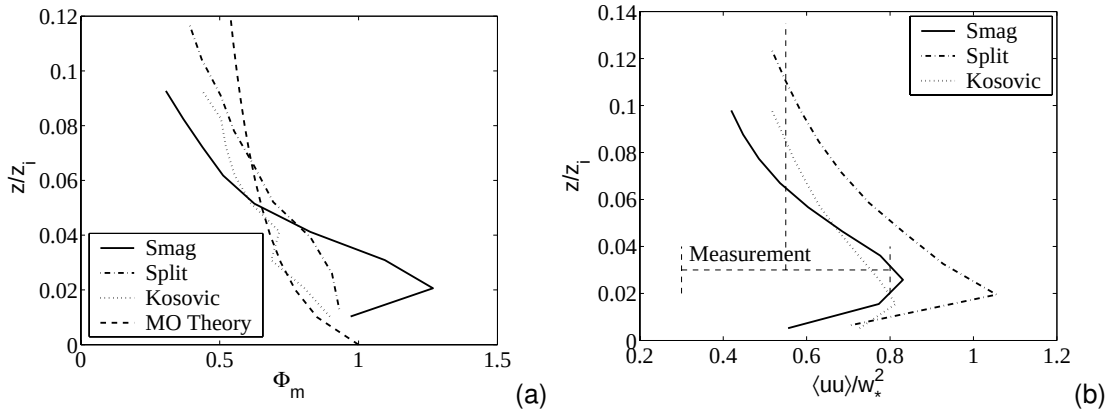

Figure 1: (a) LES results of the mean vertical gradient of the horizontal resolvable-scale velocity in the surface layer. The dashed line is the empirical form based on the the Monin-Obukhov similarity theory (Businger *et al.* 1971); b) LES results of the horizontal velocity variance and the Minnesota measurements (Wyngaard (1988)) with an error bar.

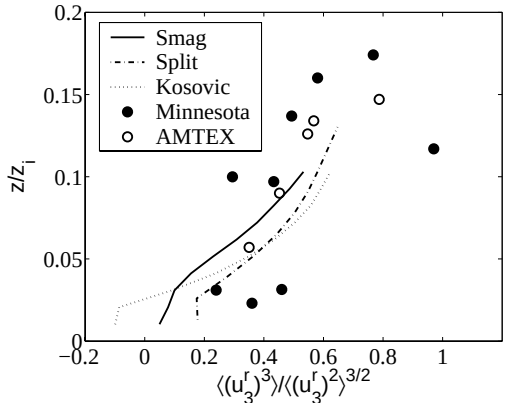

Figure 2: LES results of the vertical resolvable-scale velocity skewness profiles in the surface layer. The solid and open circles are from the Minnesota experiment (Wyngaard 1988) and AMTEX (Lenschow and Stephens (1980)), respectively.

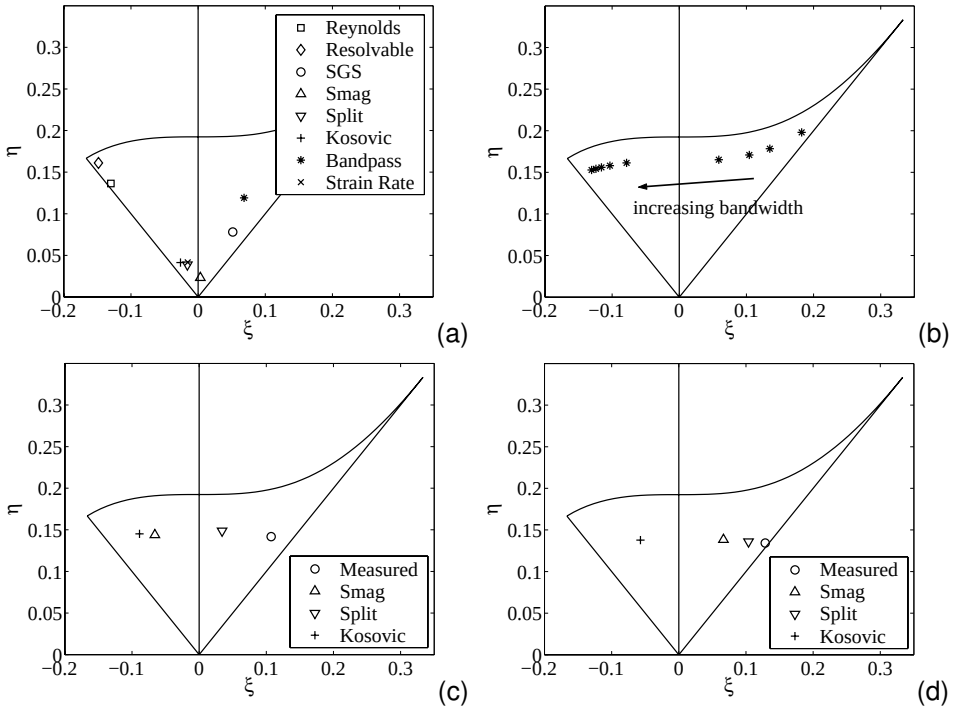

Figure 3: Lumley triangle representations of: a) the measured Reynolds stress, mean resolvable-scale stress, mean SGS stress, mean band-passed stress with a second filter size twice that of the first filter, and the modeled (*a priori* test) mean SGS stress. The strain rate is also given for reference. b) the LES results of the mean band-passed stress using the Kosović model. The bandwidth increases from 2 grid spaces to 34 grid spaces with an increment of 4 grid spaces; c) the measured and the modeled (*a priori* test) mean SGS stress production rate $\langle P_{ij} \rangle$; d) the measured and the modeled (*a priori* test) $\langle P_{ij}^d \rangle$.

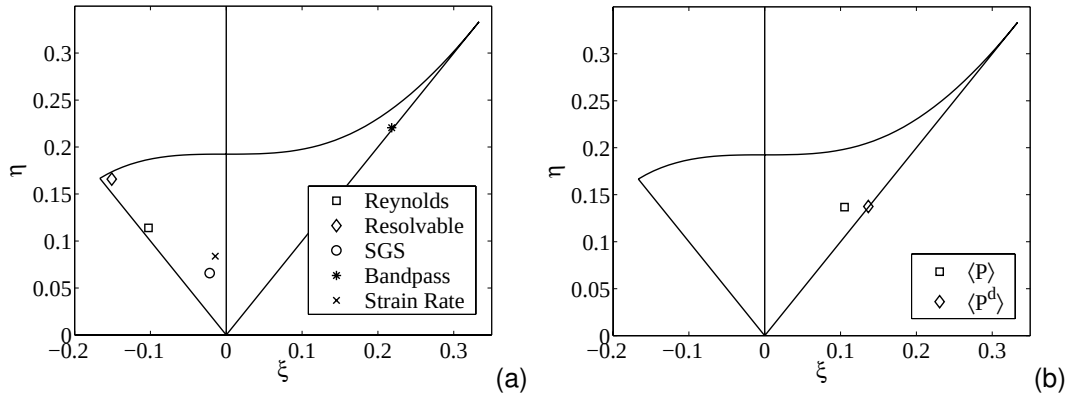

Figure 4: The Smagorinsky model results (*a posteriori* test) of the Lumley triangle representations of: a) the Reynolds stress, mean resolvable-scale stress, mean SGS stress, mean band-passed stress with a second filter size twice that of the first filter, and the mean strain rate; b) the mean SGS stress production rate.

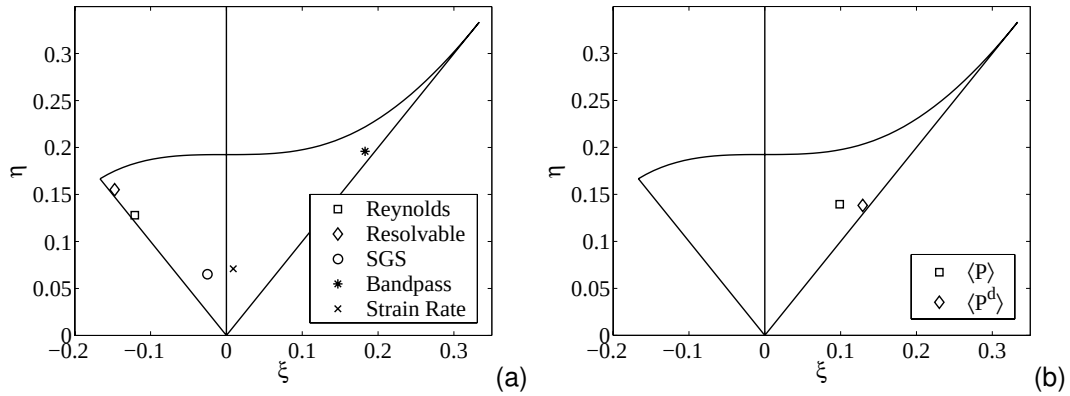

Figure 5: The split model results (*a posteriori* test) of the Lumley triangle representations of: a) the Reynolds stress, mean resolvable-scale stress, mean SGS stress, mean band-passed stress with a second filter size twice that of the first filter, and the mean strain rate; b) the mean SGS stress production rate.

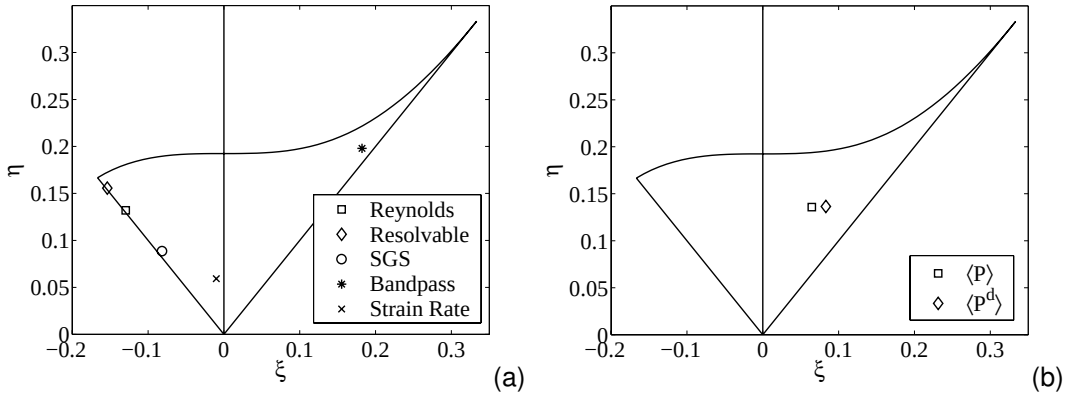

Figure 6: The Kosović model results (*a posteriori* test) of the Lumley triangle representations of: a) the Reynolds stress, mean resolvable-scale stress, mean SGS stress, mean band-passed stress with a second filter size twice that of the first filter, and the mean strain rate; b) the mean SGS stress production rate.

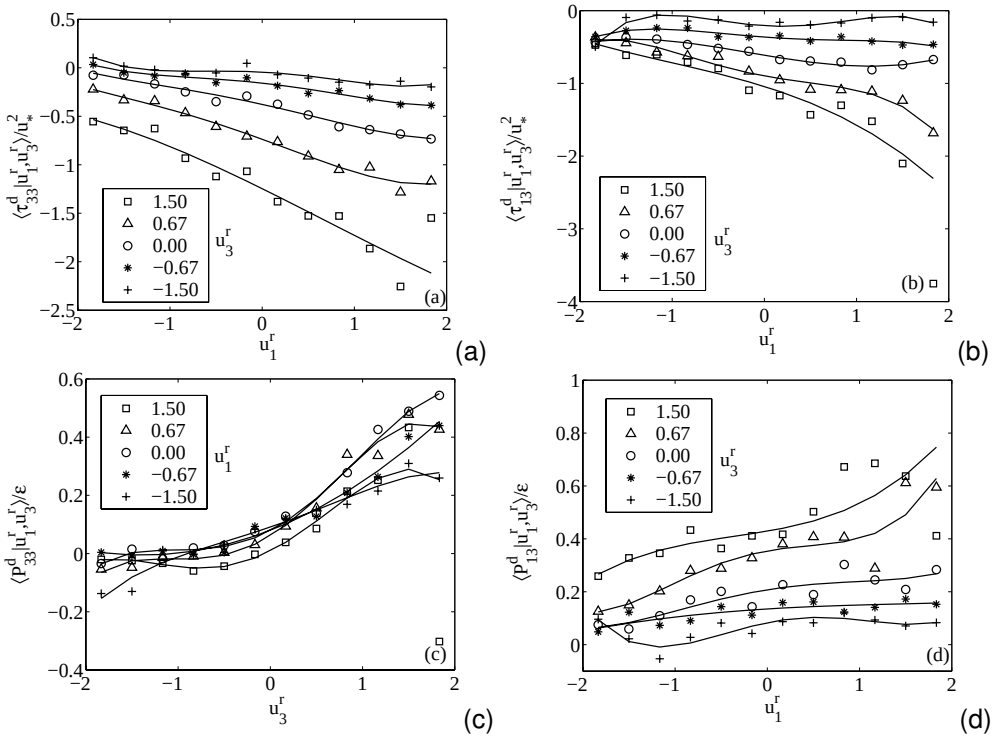

Figure 7: Conditional means of the measured deviatoric SGS stress components and its production rate conditional on the resolvable-scale velocity components. The dependence on the horizontal velocity components is generally stronger for positive u_3^r.

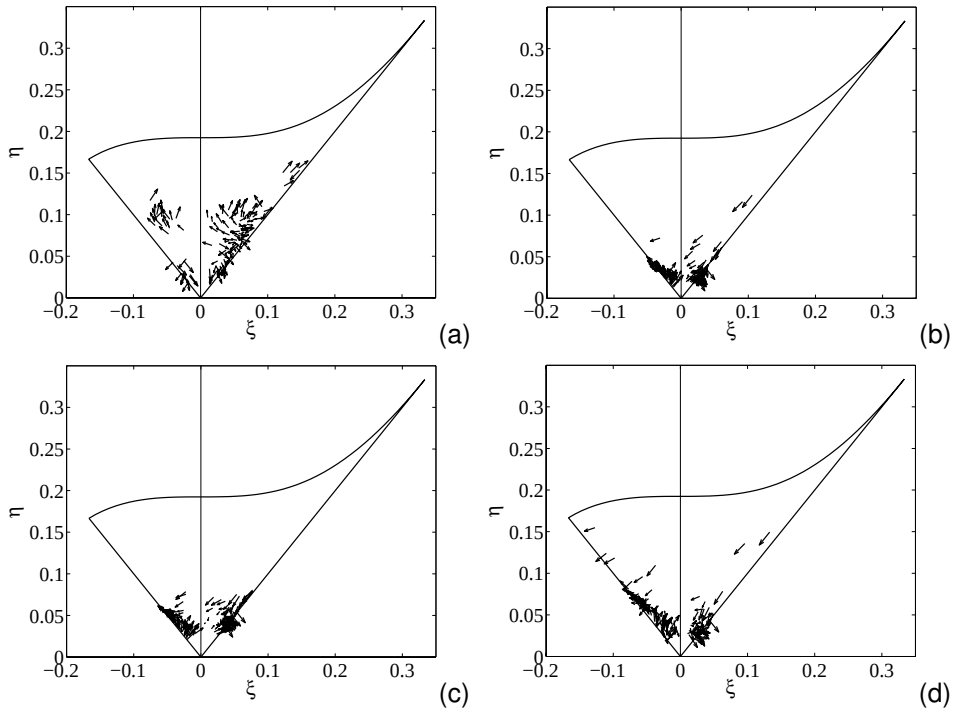

Figure 8: Lumley triangle representations of the measured and modeled (*a priori* test) conditional SGS stress: a) the measurements; b) the Smagorinsky model; c) the split model; d) the Kosović model. The arrows represent the conditioning vector (u_1^r, u_3^r).

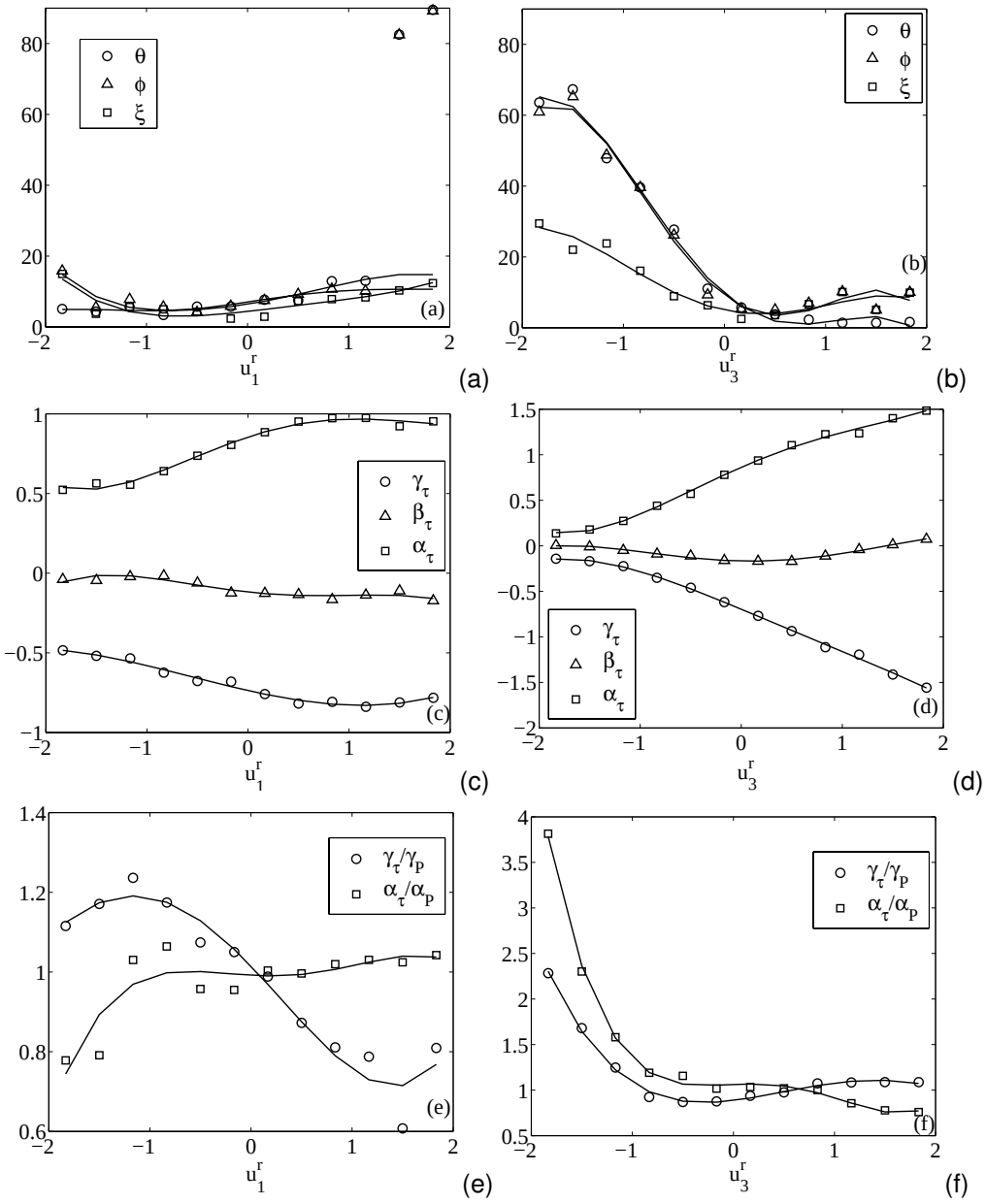

Figure 9: The measured geometric alignment angles and eigenvalues of the conditional SGS stress and its production rate: (a-b) the geometric alignment angles; (c-d) the eigenvalues of the conditional SGS stress; (e-f) the eigenvalue ratios of the conditional SGS stress to its production rate.

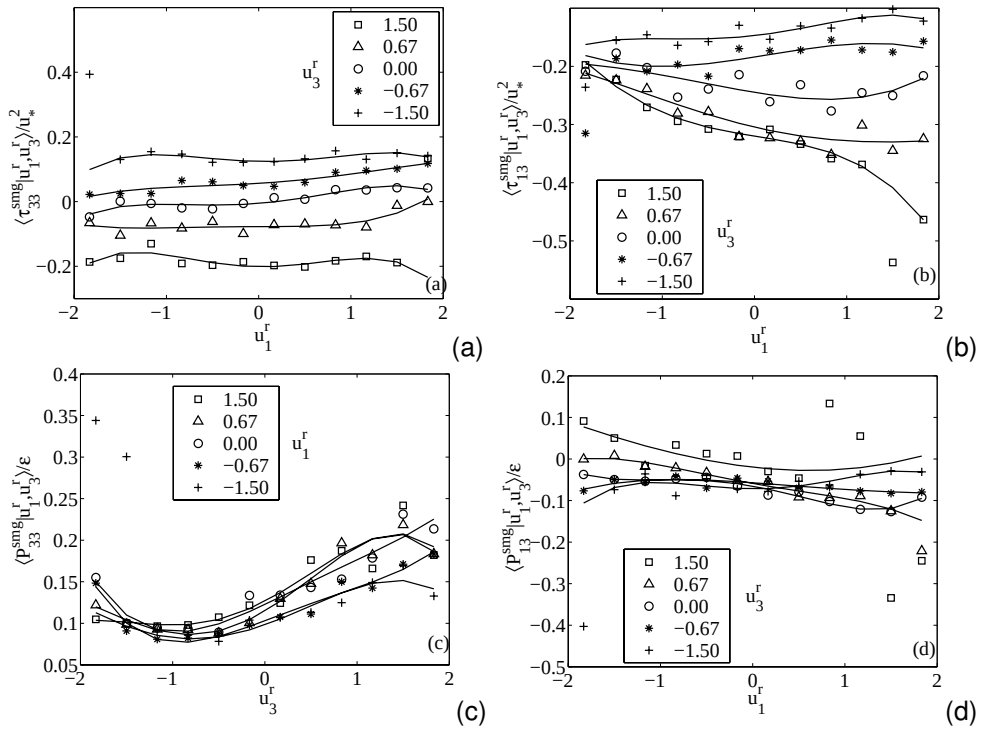

Figure 10: Modeled conditional SGS stress and its production rate (*a priori* test) using the Smagorinsky model. Only the trend of $\langle \tau_{13} | u_1^r, u_3^r \rangle$ is predicted reasonably well.

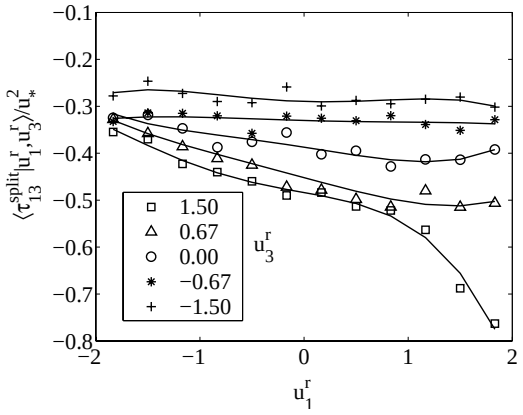

Figure 11: Modeled conditional SGS shear stress (*a priori* test) using the split model. The variations of the predicted $\langle \tau_{13} | u_1^r, u_3^r \rangle$ are smaller but the magnitude is larger than that of the Smagorinsky model due to the contribution from the mean part.

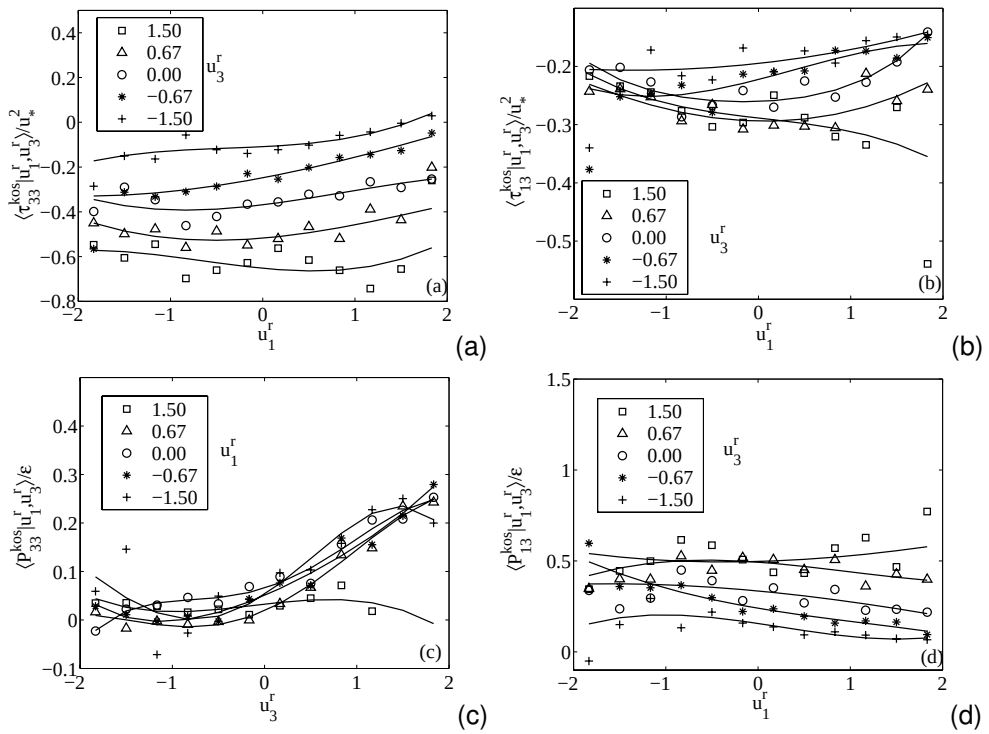

Figure 12: Modeled conditional SGS stress and its production rate (*a priori* test) using the Kosović model.

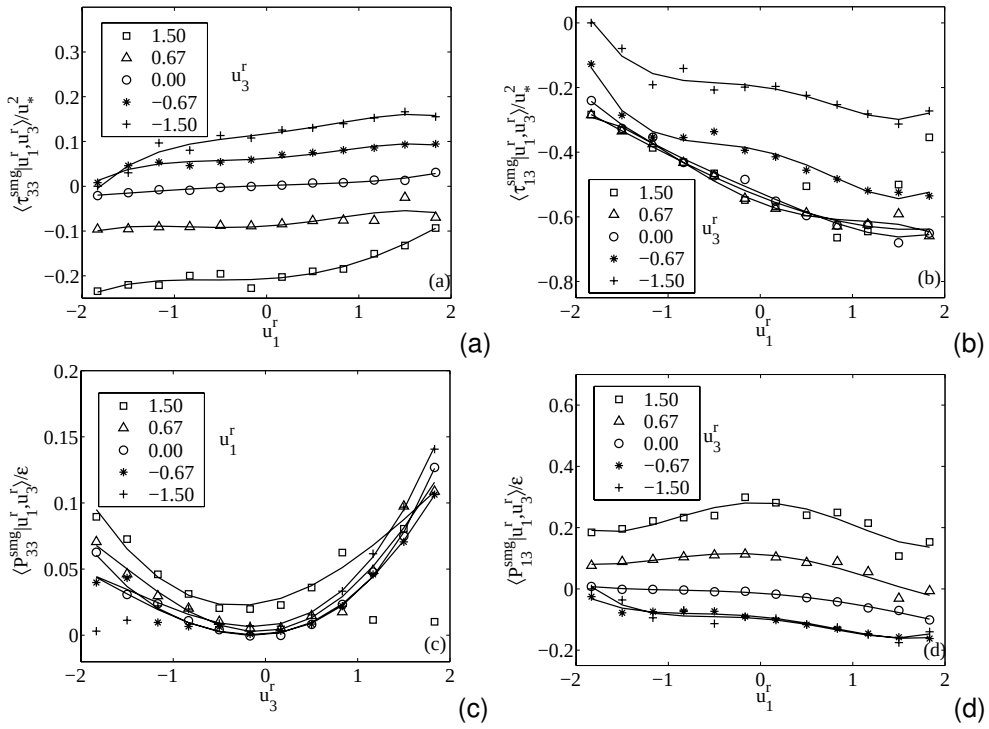

Figure 13: The Smagorinsky model results (*a posteriori* test) of the conditional SGS stress and its production rate.

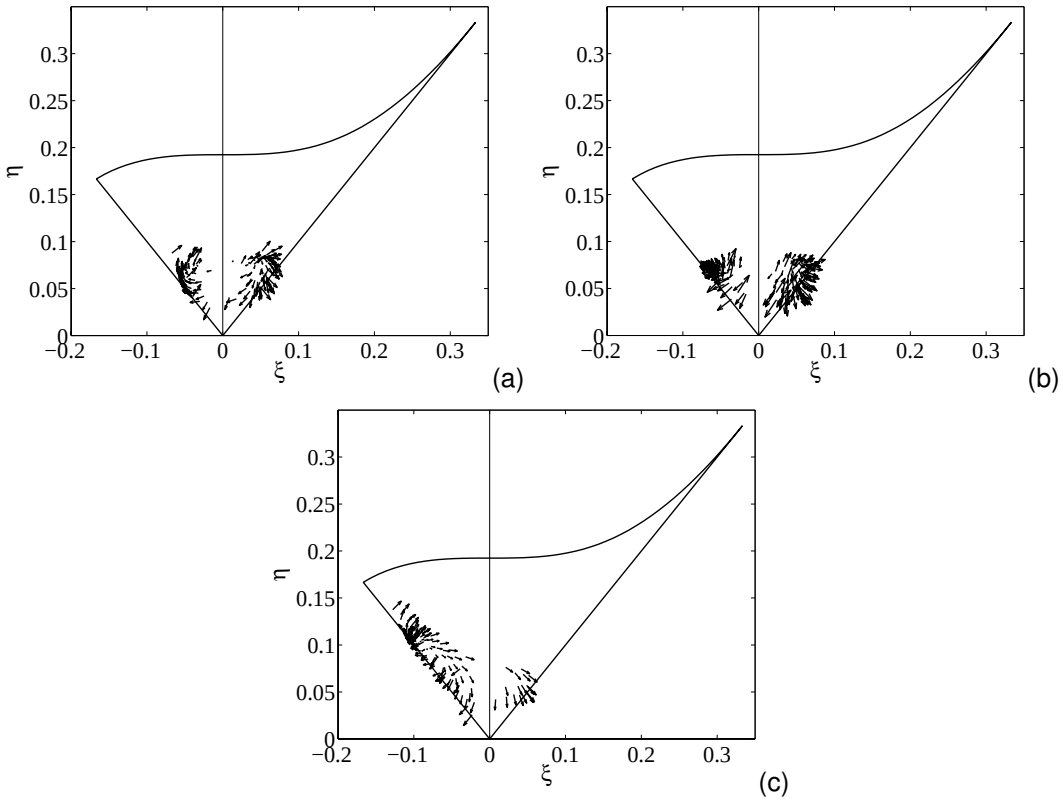

Figure 14: LES results (*a posteriori* test) of the Lumley triangle representation of the conditional SGS stress using: a) the Smagorinsky model; b) the split model; c) the Kosović model.

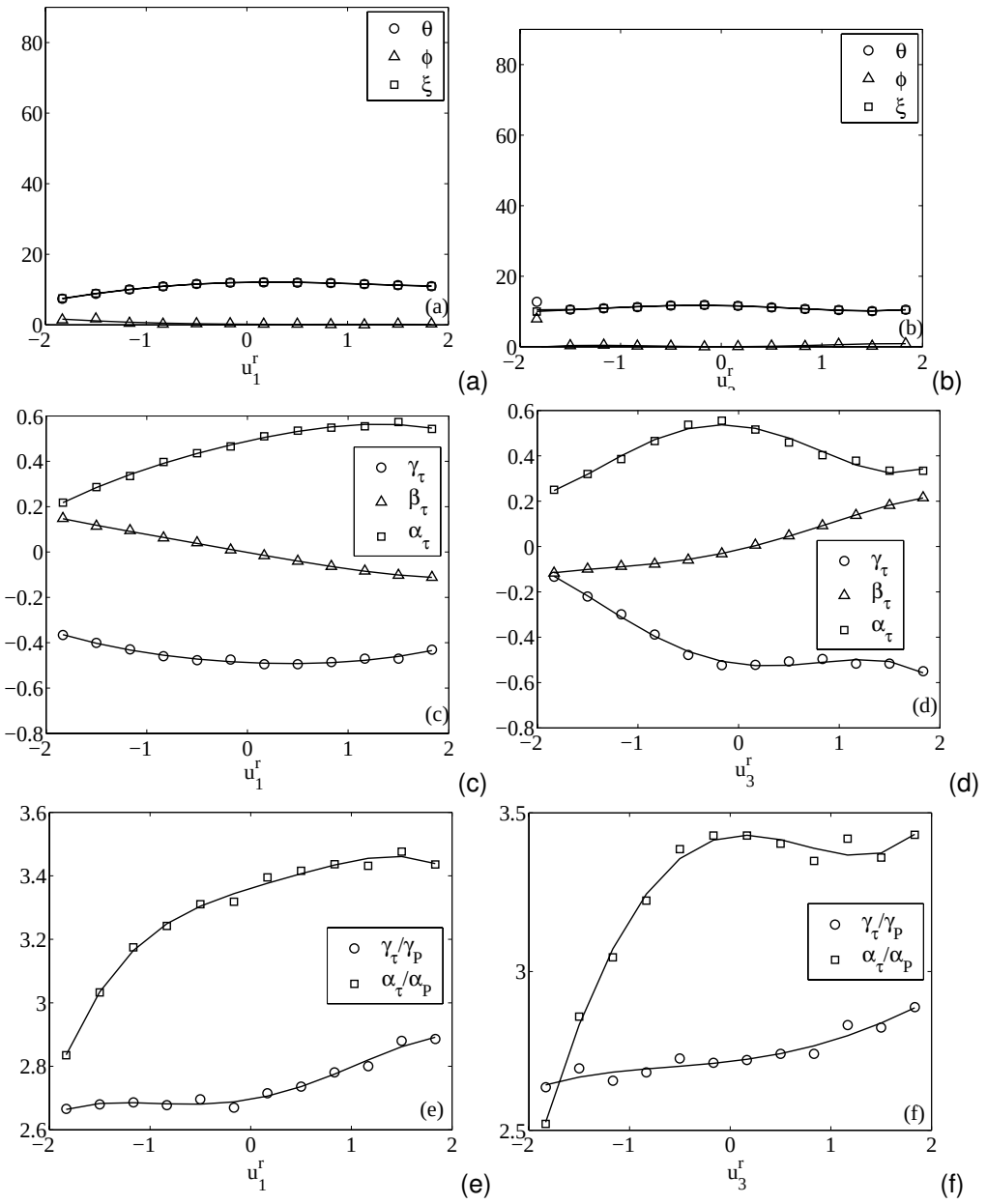

Figure 15: The Smagorinsky model results (*a posteriori* test) of the geometric alignment angles and eigenvalues of the conditional SGS stress and its production rates: (a-b) the geometric alignment angles; (c-d) the eigenvalues of the conditional SGS stress; (e-f) the eigenvalue ratios of the conditional SGS stress to its production rate.

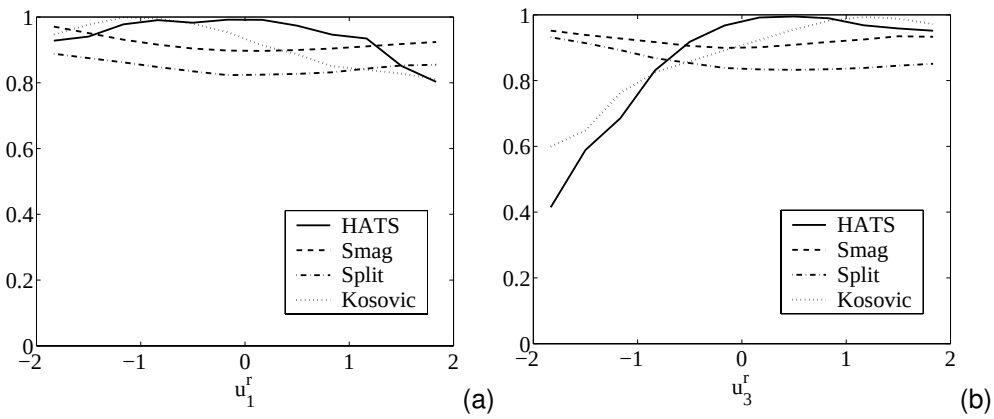

Figure 16: Contraction of the conditional SGS stress and its production rate from the LES (*a posteriori* test) and the measurements.

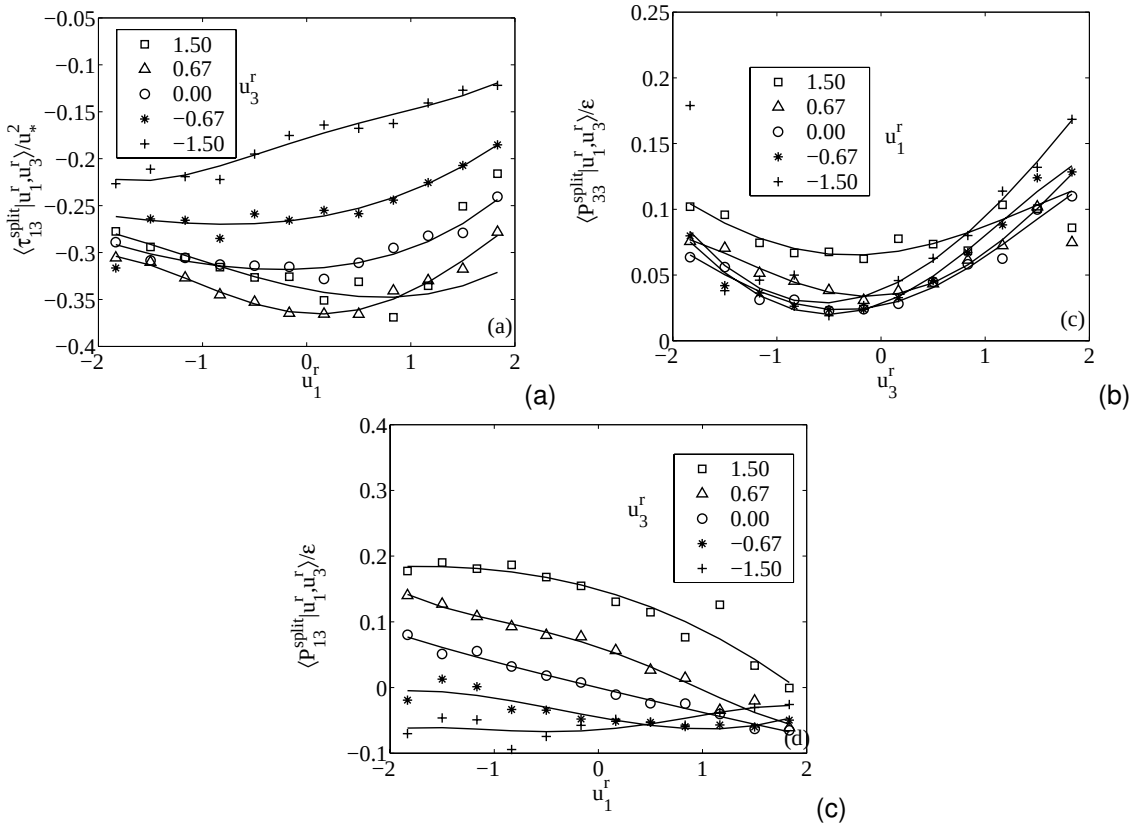

Figure 17: The split model results (*a posteriori* test) of the conditional SGS stress and its production rate.

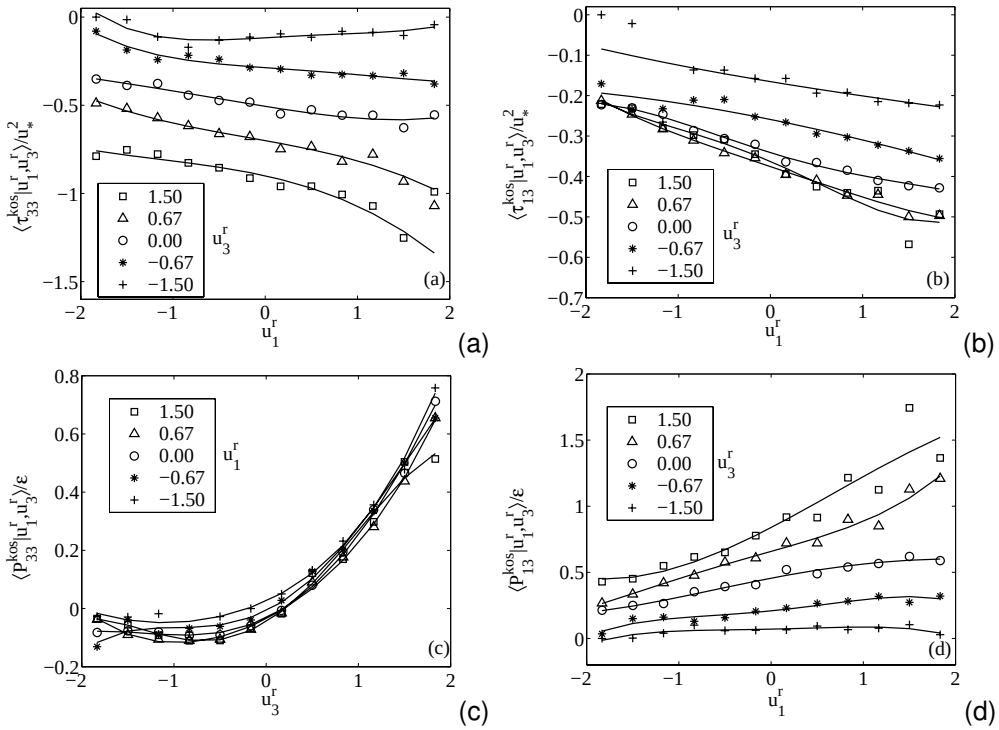

Figure 18: The Kosović model results (*a posteriori* test) of the conditional SGS stress and its production rate.

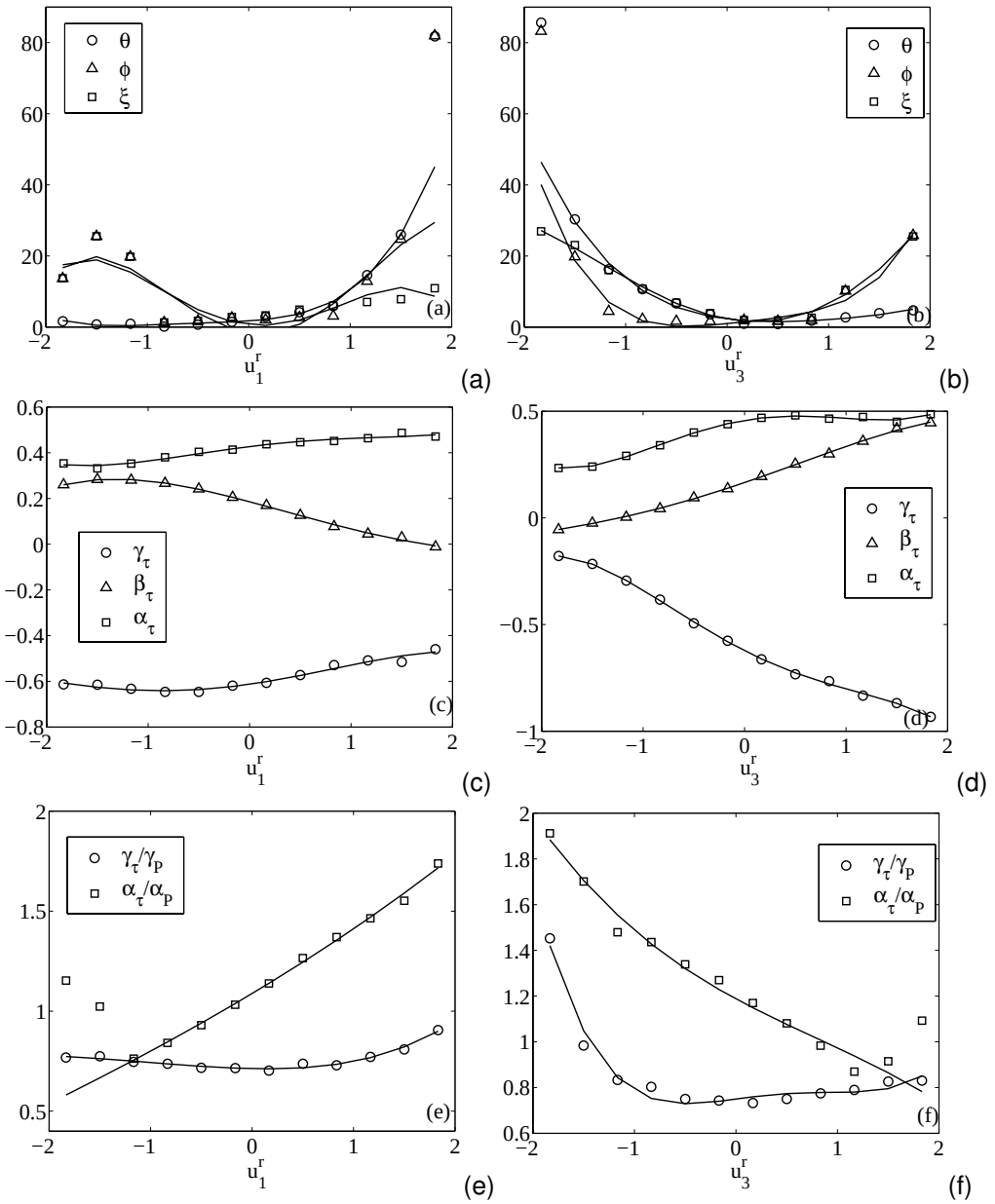

Figure 19: The Kosović model results (*a posteriori* test) of the geometric alignment angles and eigenvalues of the conditional SGS stress and its production rate: (a-b) the geometric alignment angles; (c-d) the eigenvalues of the conditional SGS stress; (e-f) the eigenvalue ratios of the conditional SGS stress to its production rate.